A repertoire of foraging decision variables in the mouse brain

Authors: Fanny Cazettes[1,b*], Masayoshi Murakami[1,2], Joao P. Morais[1], Alfonso Renart[1,a*], Zachary F. Mainen[1,a*]

[1] Champalimaud Foundation, Lisbon, Portugal.
[2] Department of Neurophysiology, University of Yamanashi, Japan.
[a] Equal contribution
[b] Lead contact

*Correspondence to:

fanny.cazettes@neuro.fchampalimaud.org,

zmainen@neuro.fchampalimaud.org,

alfonso.renart@neuro.fchampalimaud.org.

ABSTRACT

In any given situation, the environment can be parsed in different ways to define useful decision variables (DVs) for any task, but the way in which this manifold of potential decision strategies is processed to shape behavioral policies is not known. We recorded neural ensembles in the frontal cortex of mice performing a foraging task admitting multiple DVs. Optogenetic manipulations revealed that the secondary motor cortex (M2) is needed for mice to use the different DVs in the task. Surprisingly, we found that, regardless of the DV best explaining the behavior of each mouse, M2 activity reflected a full basis set of computations spanning a repertoire of DVs extending beyond those useful for the present task. Random DVs with similar temporal structure were not represented in M2, suggesting that its representational capacity is vast, but not universal. This form of multiplexing may confer considerable advantages for learning and adaptive behavior.

INTRODUCTION

An adaptive strategy to control behavior is to take actions that lead to good outcomes given that the environment is in a particular state. Yet, environmental states are often complex, with manifold sources of potentially relevant information, some that are directly observable and others that can only be revealed through a process of inference. Therefore, an agent typically also faces the problem of selecting which are the environmental variables on which to base a decision and how must these variables be processed algorithmically to reveal the appropriate 'decision variable' (DV). The problem of selecting a DV is likely a more difficult computational problem faced by a decision maker than the decision itself, but how it is accomplished has received scant investigation[1].

An important possibility is that an agent need not commit to a particular DV but may entertain several in parallel. The ability to parallelize operations of decision processing, such as temporal integration, would permit adaptation to changes in task contingencies without implementation of new computations, and could therefore potentially speed learning and provide flexibility in combining and switching of strategies. However, little is known about the limitations and possibilities for multiplexing the algorithms used to derive DVs from sensory evidence. On the one hand, behavioral studies in humans suggested that two streams of sensory evidence can only be incorporated into a DV one at a time, necessitating serial processing[2–4]. On the other hand, it has been shown that there exist neurons integrating evidence about a single sensory event with diverse timescales[5], and that diverse time-scales are present in neurons within local circuits[6], which could reflect a simple form of algorithmic multiplexing. It thus remains unclear whether various computations can be carried out in parallel on different streams of evidence to form a broad range of simultaneously available DVs.

From a theoretical standpoint, recurrent neural networks have been shown to provide useful descriptions of decision-making in frontal and motor cortical networks[7,8]. Such networks have the ability to compute high-dimensional representations of inputs that allow simultaneous decoding of multiple relevant readouts, including the ability to combine inputs experienced at different moments in time[9–12]. Transformers are another example of an architecture for parallelization that can achieve faster and more flexible learning on sequential data[13,14]. Yet, there is still little known about how the brain might multiplex computations on temporally extended data streams.

To directly study the possibility of multiplexing computations on sequential inputs in the brain, we leveraged a foraging task based on processing a stream of binary outcomes (successful and unsuccessful foraging attempts) to inform a decision of whether to leave or stay[15,16]. This task admits multiple strategies for processing the series of outcomes which are associated with

different precisely quantifiable DVs. Evaluation of these DVs allows the experimenter to infer the implementation of 'counterfactual' strategies, i.e., strategies which are potentially applicable, but unused. This can be done because the task involves precise sequences of stimuli that can be processed in multiple ways. If such counterfactual strategies could be decoded from the brain, it would be evidence for parallel processing of serial information.

In previous work, it was found that mice could make decisions to leave a foraging site based on a variable that embodies an inference about a hidden state (indicating that resources at the current foraging site are still available), which has been termed “inference-based” strategy. Alternatively, decisions can be based on a running estimate of how much reward mice have recently experienced at the site, which has been termed a “stimulus-bound” strategy[16]. From a purely computational point of view, however, these two ways of processing reward information share some similarities. Both strategies critically rely on temporal accumulation of evidence about the relevant action outcomes[16–18], and they differ in that the inference-based strategy requires an additional computation (i.e., the reset of an accumulated count). More generally, these two types of strategies could potentially be unified based on a common set of primitives which would form a basis set for an even larger set of processing strategies. If this were the case, then we might actually expect to see both strategies, and others, encoded in parallel within the same brain region.

Here, using population recordings and optogenetic silencing in the frontal cortex of mice performing the foraging task, we identified a brain region (the secondary motor cortex) where DVs corresponding to multiple strategies could be decoded simultaneously. Critically, although different mice across different sessions alternated in which strategy they used, we found that the extent to which each DV was represented in the cortex did not depend on the particular strategy used by each mouse. We next formulated a generative model of foraging decisions, named the FORAGE model, which could produce a larger repertoire of DVs of which the two just highlighted were particular examples. We found that the whole repertoire of DVs produced by the FORAGE model, but not arbitrary DVs, could be simultaneously and independently decoded from neural ensembles in the same region. Overall, these observations suggest that mice use a multiplexed algorithm for decision-making that relies on the parallel computation of multiple DVs in the frontal cortex and provide evidence for the use of a specific basis set that appears to be applied to the ethologically critical problem of foraging.

RESULTS

Multiple DVs predict leaving behavior

In our task, a head-fixed mouse collected rewards at a virtual foraging site by licking from a spout (Fig. 1a; Supplementary Fig. 1). During a foraging bout, either a fixed amount of reward (1μL consumed in a single lick) or nothing was delivered for each detected lick. At any time, the mouse could choose to continue licking or give up and explore a new site by starting to run. In particular, there were two virtual foraging sites only one of which was active at a given time and would deliver reward with a probability of 0.9 after each lick. The active site had also a probability of 0.3 of switching after each lick. This switch from active to inactive only happened once while the mouse was at the site, so if it left the site before the switch, no rewards were delivered at the other site (and it had to return to the original site and restart licking). Therefore, the best strategy to time the leaving decision was to infer the latent state corresponding to which port was currently active[16]. This inference-based strategy was supported by a particular DV that consisted of temporally accumulating consecutive failures with a complete reset upon receiving a reward (Fig. 1b). This is because a failure to receive reward provides evidence that the active state had switched, whereas a reward always signaled the active state with certainty. Using this strategy, mice would leave the current site when the *'consecutive failures'* DV reaches a given threshold[16]. Yet, in principle, mice could time their decision to leave by using any number of alternative strategies based on the sequence of rewarded and unrewarded licks regardless of the true causal structure of the task. In fact, early on during training when learning the task, mice do not appear to calculate the inference-based DV[16]. Their behavior is better described by a strategy which does not contemplate discrete transitions to a fully depleted state, and instead relies on a running estimate of the '*value'* of the current site based on the difference between recently observed rewards and failures (Fig. 1c). Using this strategy, mice decide to abandon a foraging site when its value is sufficiently low (or its negative sufficiently high). We refer to this as a *stimulus-bound strategy* because it treats observable outcomes (the stimuli) as direct – although probabilistic – reporters of the valence of current environmental states, without further assumptions or models about environmental dynamics. For our present purposes, the essential aspect of these two strategies is that they use the same observable outcomes (series of rewarded and unrewarded licks) in qualitatively different ways to update their corresponding DV – a full reset versus a quantitative incremental increase in current value. This allows us to unambiguously identify the two DVs, their behavioral consequences, and their neural representations.

After several days of interaction with this setup (n = 13 ± 5 days; mean ± s.d.), mice (n = 21) learned to exploit each site for several seconds (Fig. 1d,e). Considering the last two sessions of training (n = 42 sessions total), we examined which strategy mice used to time their leaving decisions. As demonstrated previously[16], for all mice the probability of leaving increased with

the number of consecutive failures (Fig. 1f). Yet, not all mice treated rewards equally. For some mice, the number of previous rewards did not affect the probability of leaving after a set number of failures (Fig. 1g, pink), consistent with the inference-based strategy. In contrast, for some other mice the number of failed attempts that they tolerated before leaving the site correlated with the number of previous rewards (Fig. 1g, blue), consistent with the stimulus-bound strategy. We quantified these effects using a linear regression model that predicted the number of consecutive failures before leaving as a function of the number of prior rewards in the current bout (Fig. 1h). We found that the regression coefficient varied strongly within our cohort, consistent with the just-described behavioral heterogeneity across sessions. The distribution across sessions showed signs of bimodality with a dip close to 0.5. Using this criterion, behavior was more consistent with the inference-based strategy in n = 23 sessions (coefficient less than 0.5) and more consistent with the stimulus-bound strategy in the remaining n = 19 sessions (coefficient larger than 0.5). To check if the heterogeneity in strategy was due to variability from session-to-session, mouse-to-mouse, or both, we examined whether the regression coefficients of each mouse varied across consecutive sessions (Fig. 1i). Overall, we observed that the majority of mice kept the same strategy across consecutive sessions (Fig. 1i, gray), but some mice (n = 4) also switched strategy from one session to the next (Fig. 1i black).

These observations indicate that mice vary in their foraging strategies across individuals and sessions, but do not directly indicate how well mice's behavior are actually described by the DVs. Therefore, we next quantified how well the different DVs 'consecutive failures' and 'negative value' could predict the precise moment (lick) when an individual mouse would switch sites on a given trial. Specifically, we used regularized logistic regression to model the probability that each lick (n = 2,882 ± 1,631 licks per session; mean ± s.d. across 42 sessions) was the last one in the bout, considering simultaneously the stimulus-bound and the inference-based DVs as predictors (Fig. 1j top, Methods). We estimated the goodness of fit of the two models using the 'deviance explained', a generalization of r-squared where '0' meant chance level and '1' meant perfect predictions. We found a median deviance explained of 0.16, a value significantly better than chance for all mice (Fig. 1k, gray box, Wilcoxon rank test: $p < 10^{-6}$). To provide a reference for the meaning of a deviance of this magnitude, we used the same logistic regression model to predict the leaving decisions of a simulated agent in which the 'ground truth' was known. For this, we simulated behavioral sessions of an agent making decisions using a logistic function and the DV of the inference strategy with equal numbers of bouts as in the real sessions. We found that the model recovered the ground truth parameters with high accuracy (Supplementary Fig. 2). Furthermore, the deviance explained of the simulated data, median = 0.25, was only slightly greater than that of the real data (Fig. 1k), indicating that the model with DVs performed close to the maximum that could be expected given the statistical nature of the task. This multivariate approach also confirmed that the two DVs were used to different extents across sessions (Fig. 1l) and, compared to the univariate regression (Fig. 1h), provided even

clearer indication of changes in dominant strategy across sessions (Fig. 1l, Supplementary Fig. 2e).

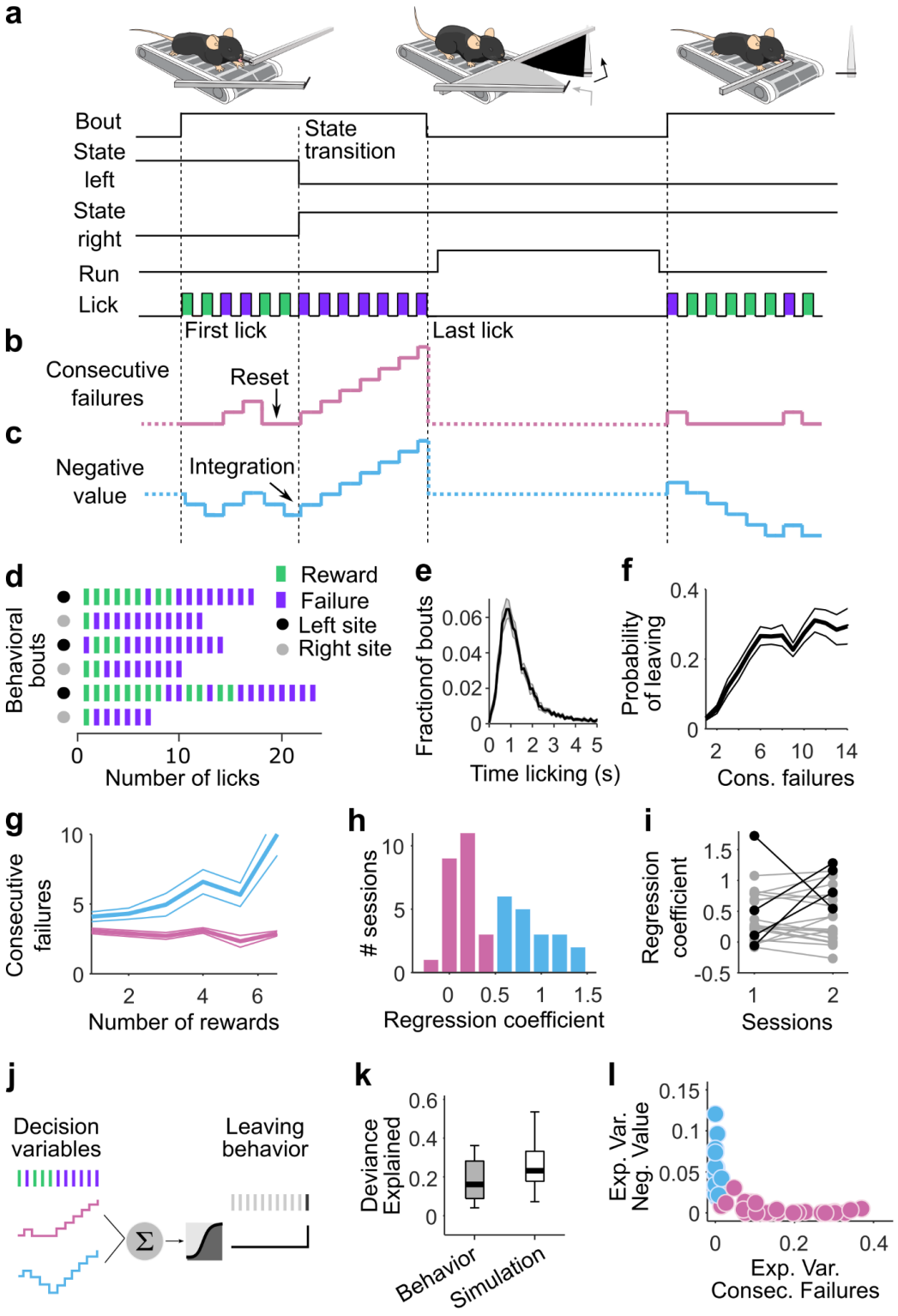

Figure 1: Multiple DVs predict foraging behavior.

(a) A head-fixed mouse placed on a treadmill chooses to exploit one of the two foraging sites (two movable arms on each side of the treadmill). A bout of behavior consists of a series of rewarded and unrewarded licks (action outcomes) at one of the sites. When a site is in an active state, the probability of each lick being rewarded is 90% and each lick is associated with a 30% probability of state transition. Independently from state transition, animals can choose to switch between sites at any time by running a set distance on the treadmill. During site-switching, the spout in front moves away and the distal one moves into place.

(b) The DV that the mouse needs to compute to infer the hidden state of the resource site.

(c) Alternative DV supporting a stimulus-bound strategy: the 'negative value'.

(d) Example sequences of observable events during different behavior bouts.

(e) Histogram of bout duration (mean ± s.e.m. across sessions; n = 42).

(f) Probability of leaving the foraging site as a function of the number of consecutive failures after the last reward (mean ± s.d. across mice).

(g) Consecutive failures before leaving as a function of reward number (mean ± s.d.) in example sessions from two different mice.

(h) Distribution of the slope coefficients of a linear regression model that predicted the number of consecutive failures before leaving as a function of the number of prior rewards. For visualization, pink are the slope coefficients close to zero (coefficient < 0.5, arbitrary threshold), while blue are sessions with positive slope coefficients.

(i) Slope coefficients from (h) between two consecutive sessions (1 and 2) for different mice. Sessions between which the coefficient values vary by more than 0.5 (arbitrary threshold) are highlighted in black.

(j) Illustration of the logistic regression model for predicting the leaving behavior of the mouse from the two different DVs.

(k) Deviance explained from the logistic regression that predicts choice behavior based on the DVs (gray box) and from simulated data where the behavior is truly inference-based (white box). On each box, the central mark indicates the median across behavioral sessions, and the bottom and top edges of the box indicate the 25th and 75th percentiles, respectively. The whiskers extend to the most extreme data points.

(l) Explained variance from the logistic regression that predicts choice behavior based on the DVs. Sessions where 'consecutive failures' is dominant (Var. Exp. Cons. Fail > Var. Exp. Neg. Value) are labeled in pink, while sessions where 'negative value is dominant' are labeled in blue (Var. Exp. Cons. Fail < Var. Exp. Neg. Value).

Neural activity related to the leaving behavior

In order to examine the neural basis of DVs underlying the leaving behavior, we first had to identify brain regions that predicted the leaving behavior. We used Neuropixels 1.0 electrode arrays[19], which are single shank probes with hundreds of recording sites that allow registering the activity of large ensembles of neurons (n = 151 ± 59 neurons per session; mean ± s.d.) in multiple regions of the frontal cortex during the task. We targeted the secondary motor cortex (M2; n = 66 ± 37 neurons per session; mean ± s.d.), thought to be important for timing self-initiated actions[20] and planning licking behavior[21], and the orbitofrontal cortex (OFC; n = 55 ± 24 neurons per session; mean ± s.d.), whose inactivation impacted the performance of inference-based decision-making in freely moving mice in the foraging task[16]. We also recorded in the olfactory cortex (Olf; n = 31 ± 23 neurons per session; mean ± s.d.), which is directly ventral to the OFC and can be accessed easily thanks to the long shank of the probe (Fig. 2a,b; Supplementary Fig. 3), but which would not be expected to be specifically involved in this task. To examine neural responses during the evidence accumulation process, we considered the momentary response patterns of isolated neurons in small time windows (Fig. 2c, Methods). Because we observed heterogeneous task-related activity in many single neurons in all regions (Fig. 2d), we focused on how population activity from each single region predicted the leaving behavior of mice (n = 11 recording sessions, 1 recording session per mouse except 1 mouse with 2 recording sessions). Using cross-validated and regularized logistic regressions, we decoded the leaving behavior (i.e., the probability that each lick was the last in the bout) from population responses around each lick (200 ms window) in each session (Fig. 2e, n = 2,533 ± 1,524 licks per session; mean ± s.d. across 11 sessions). To allow for a fair comparison between brain regions, we controlled for the different number of recorded neurons in each region by using as predictors only the first N principal components of neural activity (M2: N = 31 ± 17; OFC: N = 29 ± 9; Olf: N = 16 ± 13) , which predicted up to 95% of its total variance (see Methods for additional control analyses). We found that the leaving behavior could be better decoded using population activity from neurons in M2 than in OFC or Olf (Fig. 2f).

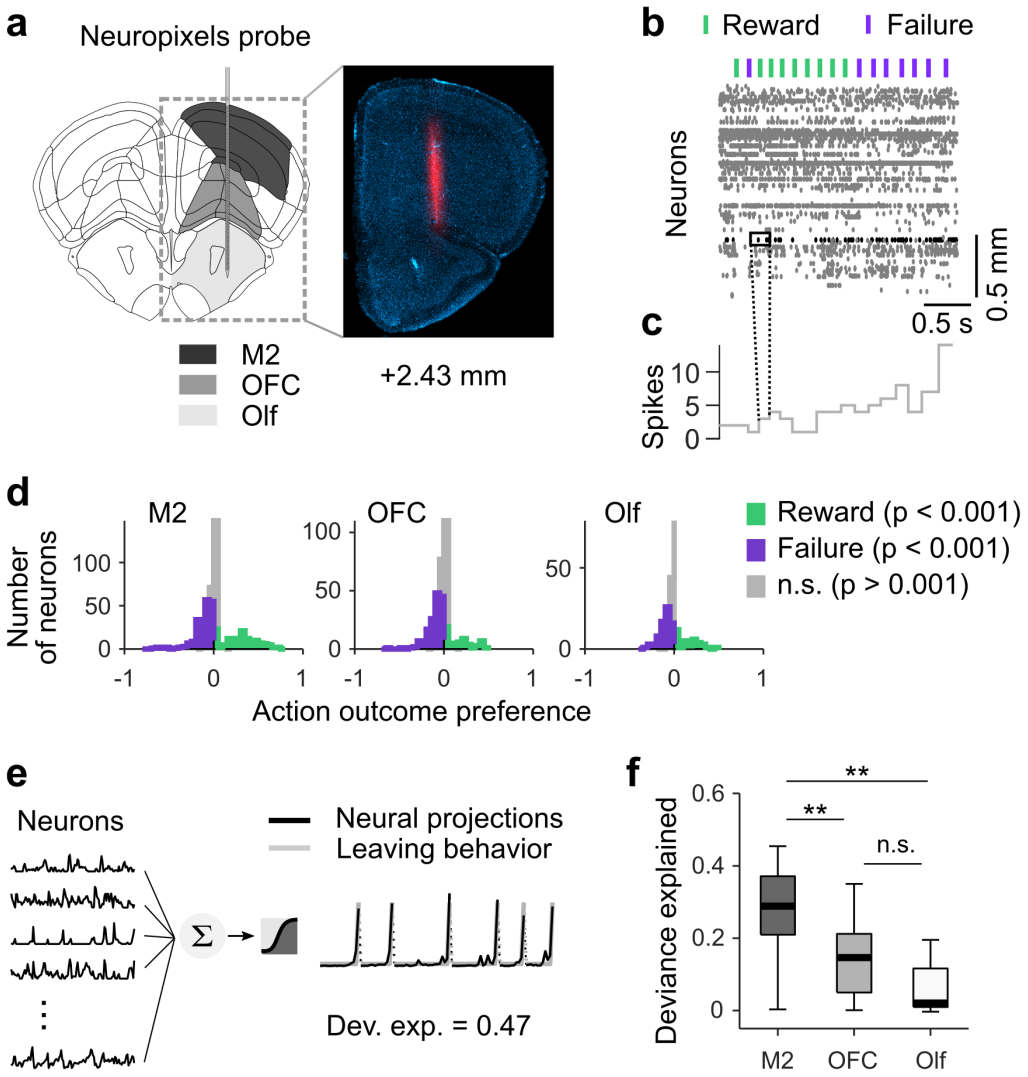

Figure 2: Neural activity related to the leaving behavior.

(a) Schematic target location of probe insertion and an example histology of electrode track. Vertical insertions were performed within a 1 mm diameter craniotomy centered around +2.5 mm anterior and +1.5 mm lateral from Bregma.

(b) Example raster plot of 140 simultaneously recorded neurons from M2. Lick-outcome times are indicated by the green (reward) and purple (failure) dashes.

(c) Binned response profile of an example neuron. For all analyses, otherwise noted, we averaged for each neuron the number of spikes into bins by considering a 200 ms window centered around each lick.

(d) Histogram of outcome selectivity of all neurons recorded M2 (left), OFC (middle) and Olf (right). We used receiver operator characteristic (ROC) analysis to assign a preference index to each neuron[22]. In brief, an ideal observer measures how well the modulation of neuronal firing can classify the outcome (reward or failure) on a lick-by-lick basis. We derived the outcome

preference from the area under the ROC curve as defined in [23]: $PREF_{R,F} = 2[ROC_{AREA}(f_R, f_F) - 0.5]$, where f_R and f_F are the firing rate distributions for trials where outcomes are reward and failure respectively. This measure ranges from −1 to 1, where −1 indicates preference for F (failure), 1 means preference for R (reward) and 0 represents no selectivity. The statistical significance of the preference index ($p < 0.001$, one-sided) was assessed via bootstrapping (1000 iterations). Violet and green bars indicate neurons where the index was significantly different from 0. In all regions, we found neurons significantly modulated by rewards and failures.
(e) Illustration of the logistic regression method for predicting the leaving behavior (gray, right) of the mouse from the principal components of neurons (black, left).
(f) Deviance explained from the logistic regression in each region. On each box, the central mark indicates the median across recording sessions, and the bottom and top edges of the box indicate the 25th and 75th percentiles, respectively. The whiskers extend to the most extreme data points. The two stars indicate a significant difference between regions (Wilcoxon signed rank test: $p = 0.0068$ between M2 and OFC; $p = 0.0049$ between M2 and Olf).

M2 is involved in the leaving behavior

The above results point to M2 as a key region for timing the leaving behavior of the mouse by relying on specific DVs. To further test the contribution of M2 to the implementation of DVs, we silenced M2 using an optogenetic strategy (as in Ref [16]). Specifically, we used VGAT-ChR2 mice, which express the excitatory opsin channelrhodopsin-2 in inhibitory GABAergic neurons, to optogenetically silence M2 bilaterally in 30% of randomly selected bouts (Fig. 3a). We examined 43 sessions from 6 mice, 4 of which were ChR2-expressing and 2 of which were control wild-type littermates implanted and stimulated in the same manner. M2 silencing caused no gross changes in motor features (Fig. 3b, left and right panels; Wilcoxon signed rank test: $p > 0.5$), but only a slight increase in the time spent at the site during inactivation of M2 (Fig. 3b, middle panel; Wilcoxon signed rank test: $p = 0.035$). Since M2 inactivation did not significantly impair the motor behavior, we tested if silencing M2 affected the use of the DVs to time the leaving decision. Thus, for each session, we used logistic regressions to estimate how well DVs predicted the decision to leave the current site during transient inactivation of M2 (Laser ON) and during control bouts (Laser OFF; Fig. 3c). We found that the inactivation of M2 significantly decreased the predictive power of the DVs (Fig. 3d,e, gray, paired-sample t-test: $p = 0.022$). The same protocol (implantation and laser stimulation) applied to control mice (wildtype littermates that express no inhibitory opsin) had no significant effect on this behavior (Fig. 3d,e, black, paired-sample t-test: $p > 0.05$). These results suggest that M2 is part of the neural pathway through which the DVs shape the behavior of the mice.

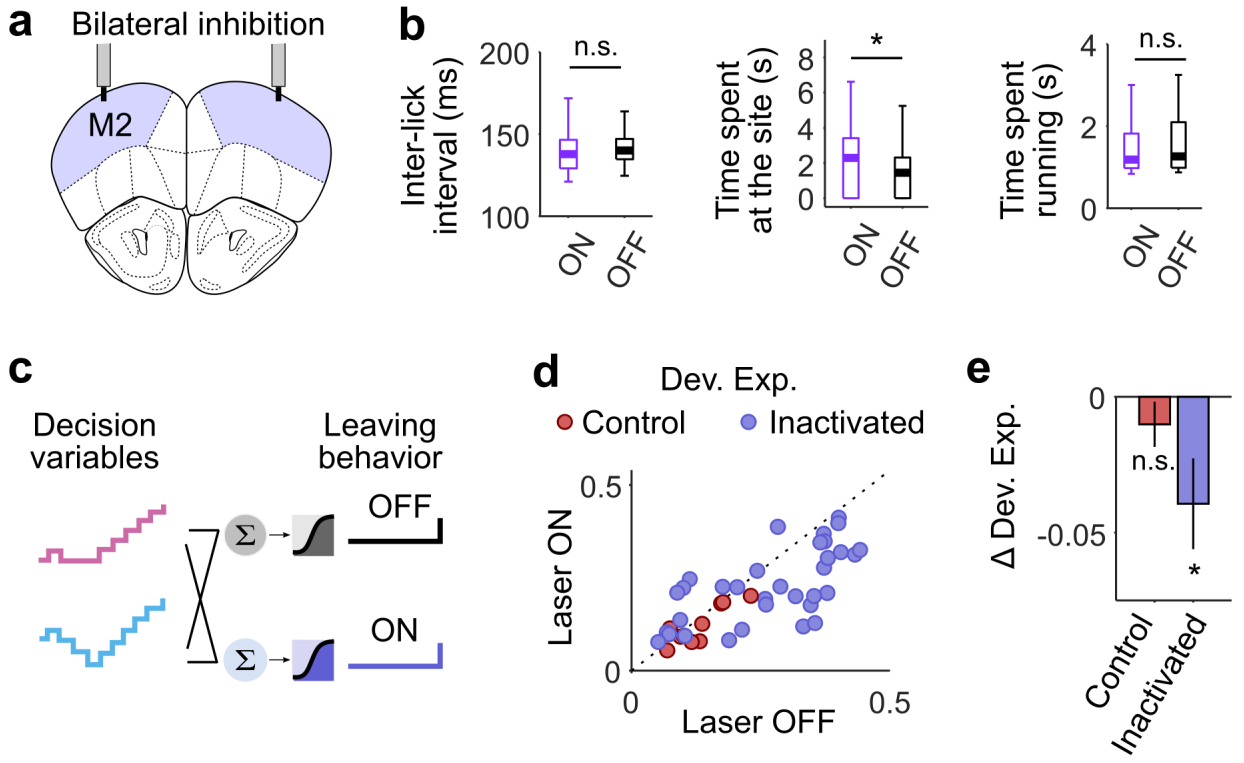

Figure 3: M2 is involved in the leaving behavior.

(a) Schematic target of optic fibers placement. Bilateral photostimulation (5 mW power per fiber, 10 ms pulses at 75 Hz) was triggered by the first lick in 30% of trials and lasted until the last lick of the bout.

(b) Left panel: the box and bars represent across-session median and 25th and 75th percentiles of the median inter-lick intervals during bouts with laser ON (violet) and laser OFF (black) of inactivated mice. Middle panel: same as in the left panel but for the time spent at a given resource site during laser ON and laser OFF bouts. Right panel: same as in the left panel but for the time spent running to switch sites after laser ON and laser OFF bouts.

(c) Illustration of the logistic regression models for independently predicting the leaving behavior of the mouse based on the DVs during photostimulation (Laser ON) and control bouts (Laser OFF).

(d) Deviance explained from the models in (b) for each session (dots) for inactivated mice (violet) and control mice (red) mice. Dots below the identity indicate the sessions where the model performed worse during photostimulation of M2.

(e) Summary statistics of the data in (d). Δ Dev. Exp. is the difference in deviance explained between Laser ON and Laser OFF (mean ± s.e.m.).

Neural representation of DVs

The inactivation experiments suggest that one might be able to read out the DV used by the mouse from M2 neural activity, and that M2 might represent this DV better than other cortical regions that afford less accurate predictions of foraging decisions. To test these ideas, we used cross-validated regression-based generalized linear models (GLM; see Methods) to decode the instantaneous magnitude of the DV associated with the behaviorally dominant strategy (i.e. the DV most predictive of behavior) – during each bout (n = 223 ± 119 bouts per session; mean ± s.d.) on a lick-by-lick basis – from the responses of neurons in each recorded brain region (Fig. 4a,b). The example data from Fig. 4a,b, which are from a single recording session during which the dominant strategy of the mouse was the inference (Var. Exp. Con. Fail. = 0.164 vs. Var. Exp. Neg. Value = 0.004), show that the related DV 'Consecutive failures' could be decoded with high accuracy from M2 activity (Dev. Exp. = 0.74). In fact, the dominant DV could be well decoded from M2 activity in all sessions (n = 11) from the different mice (Fig. 4c, black). The decodability of dominant DVs was significantly lower in other cortical regions (Fig. 4c; Wilcoxon signed rank test: $p < 10^{-3}$ between M2 and OFC; $p < 10^{-3}$ between M2 and Olf), consistent with the poorer decoding of leaving time in other areas (Fig. 2).

Since we have shown that different mice can rely on different DVs and individual mice can change decision strategies across sessions (Fig. 1), we next asked whether session-by-session heterogeneity in decision strategy could be explained by the degree to which M2 neurons reflected the DVs in a given session. Here, we used the GLM to compare the decoding of the dominant and the alternative DVs from M2 neurons in each recording session (Fig. 4a,d). Contrary to our expectation, we found that decoding was actually similar between the dominant and alternative decision-strategies. For instance, in the example session of Fig. 4a,b,d, despite the selectivity of the behavior for inference-based decisions, the DV supporting the stimulus-bound strategy could also be well decoded from M2 (Dev. Exp. = 0.41). This finding was consistent across our experiments: in all sessions, both DVs could both be read out from M2 activity (Fig. 4e; Supplementary Fig. 4). On average, the 'Consecutive failures' DV was somewhat better represented than the 'Negative value' (Wilcoxon signed rank test: $p < 10^{-3}$). This average difference could stem from the fact that the majority of mice (8 out of 11) used the inference-based strategy that relies on the 'Consecutive failures'. Thus, to test whether the DV that was most predictive of the leaving behavior was also the one that was better decoded from M2 on a session-by-session basis, we predicted the decision to leave the site from each DV (Fig. 4f) and compared the accuracy of this prediction to the accuracy of the neural representations of the DVs (Fig. 4g). There was no correlation between how M2 represented each DV in a session and how well the DV predicted behavior in the same session ($r^2 < 10^{-3}$, $p = 0.9$). Therefore, together these analyses suggest that although M2 neural activity is important to the execution of a decision strategy (Fig. 3), the pattern of neural activity in M2 is not adapted to represent

specifically the DV executed by the mouse, and instead reflects a broader range of decision strategies even when they are not currently used.

To further characterize the multiplexing of DVs in M2, we asked whether different variables are supported by distinct or overlapping populations. In particular, we examined the weights assigned to each neuron when decoding the 'Consecutive failures' vs. the 'Negative value' (Fig. 4h). We found that decoding weights for both DVs were strongly correlated (Pearson coefficient = 0.56, $p < 10^{-4}$), indicating a considerable overlap between the populations of M2 neurons that supported each DV, as opposed to compartmentalization into distinct populations for each variable.

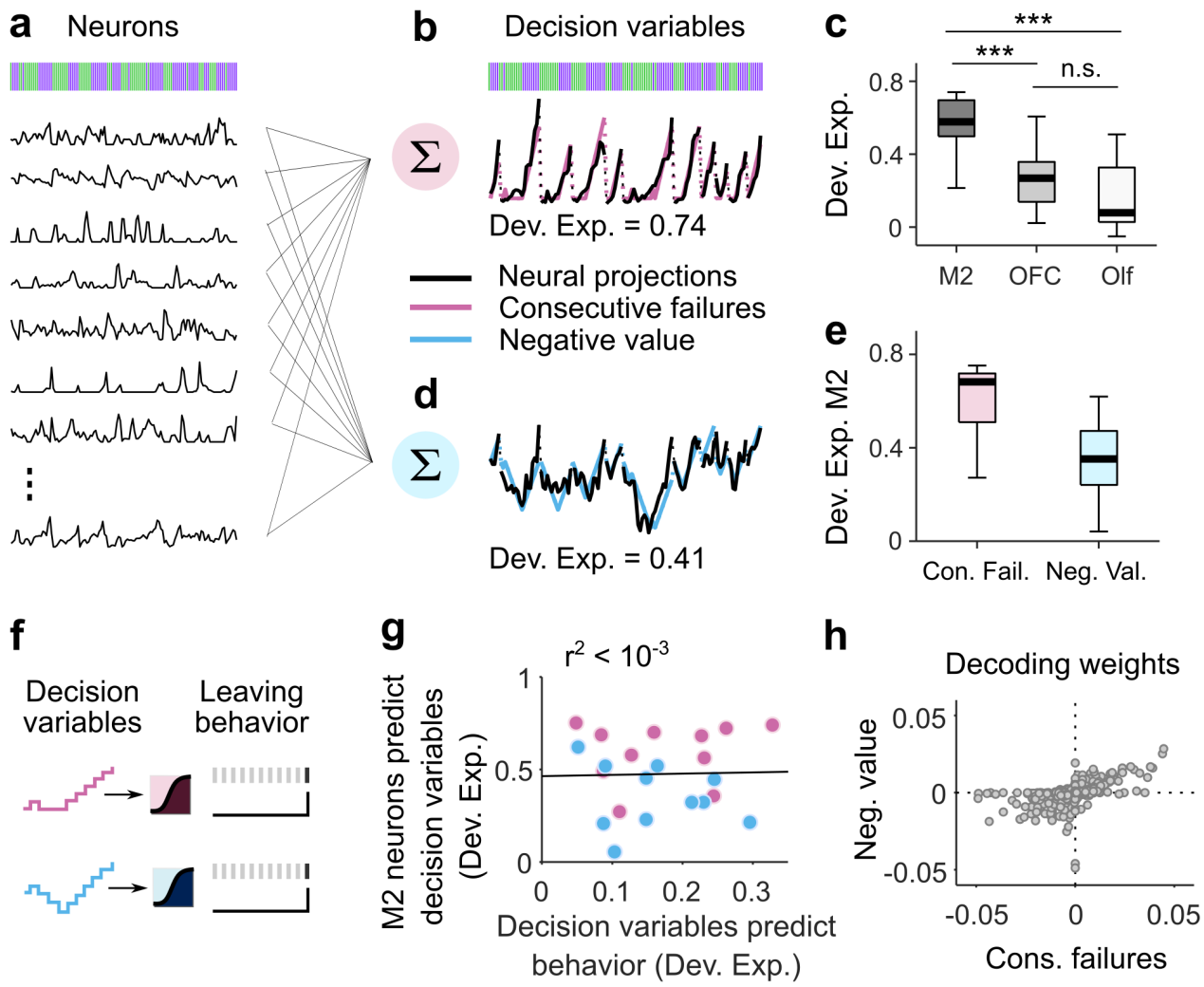

Figure 4: Neural representation of DVs.
(a) The regression models take as predictors the activity of simultaneously recorded neurons (black traces) and derive a set of decoding weights to predict the DV.
(b) Predictions of the model (black trace is the weighted sums of neural activity) overlaid onto the 'Consecutive failures' DV (pink trace).
(c) Deviance explained across sessions (median ± 25th and 75th percentiles) from the model in (a,b) in each cortical region. The stars indicate the significance of Wilcoxon signed rank test ($p < 0.001$).
(d) Predictions of the model (black trace is the weighted sums of neural activity) overlaid onto the 'Negative value' DV (blue trace).
(e) Deviance explained across sessions (median ± 25th and 75th percentiles) predicted from M2 neurons for each DV.
(f) Illustration of the logistic regression methods for predicting the leaving behavior of the mouse from each DV separately.
(g) Correlation between the neural representations of different DVs (color coded as in b,d) and how well each DV predicts behavior. Each dot corresponds to a particular DV from a given recording session. The linear regression is reported in black.
(h) Decoding weights of each M2 neuron (gray dots; total across recording $n = 778$) for the two different DVs.

Independent and simultaneous representations of DVs
A possible concern with the interpretation that M2 multiplexes actual (used) and 'counterfactual' (unused) DVs is that alternative DVs might be decodable only by virtue of being similar to the one reflected behaviorally. Although the computations underlying the two DVs are different, for the particular sequences of rewards and failures experienced by the mice, the DVs themselves are indeed fairly correlated overall (Pearson coefficient: 0.79 ± 0.15; mean ± s.d.).

As a strategy to overcome this limitation, we took advantage of the previously noted fact that the two different DVs being considered are the same in the way they treat failures but differ in the way that they treat rewards: while the 'negative value' requires negative integration of rewards, the 'consecutive failures' variable requires a complete reset by a single reward (Fig. 5a). Analysis of subsets of sequences that consist of multiple consecutive rewards should therefore reveal the differences between the two DVs (Fig. 5b). To test this, we sub-selected lick sequences and sorted them according to the relative number of rewards and failures. This produced subsequences with varying degrees of correlation between the two decision-variables (Fig. 5c). We then ran the same decoding analyses as before on these subsequences of M2 activity. We found that coding was actually independent of their degree of correlation (Fig. 5d., one-way ANOVA for each sequence across correlation values followed by multiple pairwise

comparison tests, all p-values > 0.05). These results establish that the ability to decode an alternative DV does not arise from the correlation from that variable with the dominant DV; the two DVs are independently decodable in M2 even during sequences of behavior in which they completely diverge.

In all these analyses, the window used to count the spikes was 200 ms centered around each lick (see Fig. 2b,c), which was a good tradeoff for including a significant number of spikes while mainly considering signals related to a single lick (since the average time between each lick was around 150 ms; Fig. 3b & Supplementary Fig. 1d). Yet a few spikes linked to the preceding or the following events could still be included in the 200 ms window, making it more difficult to evaluate the contribution of momentary evidence. Therefore, we tested whether both DVs remained decodable in M2 even when we strictly excluded all spikes from neighboring events by using smaller analysis windows (Fig. 5e). We found that the decodability of the DVs in M2 did not depend on the size of the window for widths larger than 20 ms (one-way ANOVA followed by multiple pairwise comparison tests, all p-values > 0.05 for windows size > 20 ms, both for 'consecutive failures' and 'negative value'), indicating that the results are not overly sensitive to the choice of parameters.

While one interpretation of multiplexing is true simultaneous representation of multiple DVs, our interpretation is relying on decoding analyses carried out over entire sessions of behavior. Could it be that multiplexing of DVs actually results from sequential switching between the two strategies within a session? To investigate this, we first examined whether there was any evidence that mice switched strategies within a session. We partitioned each session into 3 epochs with equal numbers of bouts and predicted the leaving behavior in each epoch as before (Fig. 1j). The predictive power of models using these session epochs (Deviance explained across epoch and session: 0.13 ± 0.05; median ± MAD) was similar to that of model using full sessions (Deviance explained across session: 0.15 ± 0.07; median ± MAD; Wilcoxon signed rank test: p = 0.468). We found that several mice did indeed switch at least once between inference-based and stimulus-bound strategies within the course of their recording session (Fig. 5f, 7 out of 11 switched between strategies). Thus, we examined whether we could decode better from M2 activity the 'negative value' DV during the stimulus-bound epochs than during the inference-based epochs (Fig. 5g blue), and the 'consecutive failures' DV during the inference-based epochs than during the stimulus-bound epochs (Fig. 5g, pink). Consistent with the whole session analysis (Fig. 4g), there were no significant differences between how well a given DV could be decoded when the mice behavior relied on it or not (Wilcoxon signed rank test: p > 0.05 for both comparisons). Although it remains possible that mice flicker between strategies on a fine time scale comparable to individual bouts, these analyses suggest that multiplexing of strategy is not due to drift in strategies within a session.

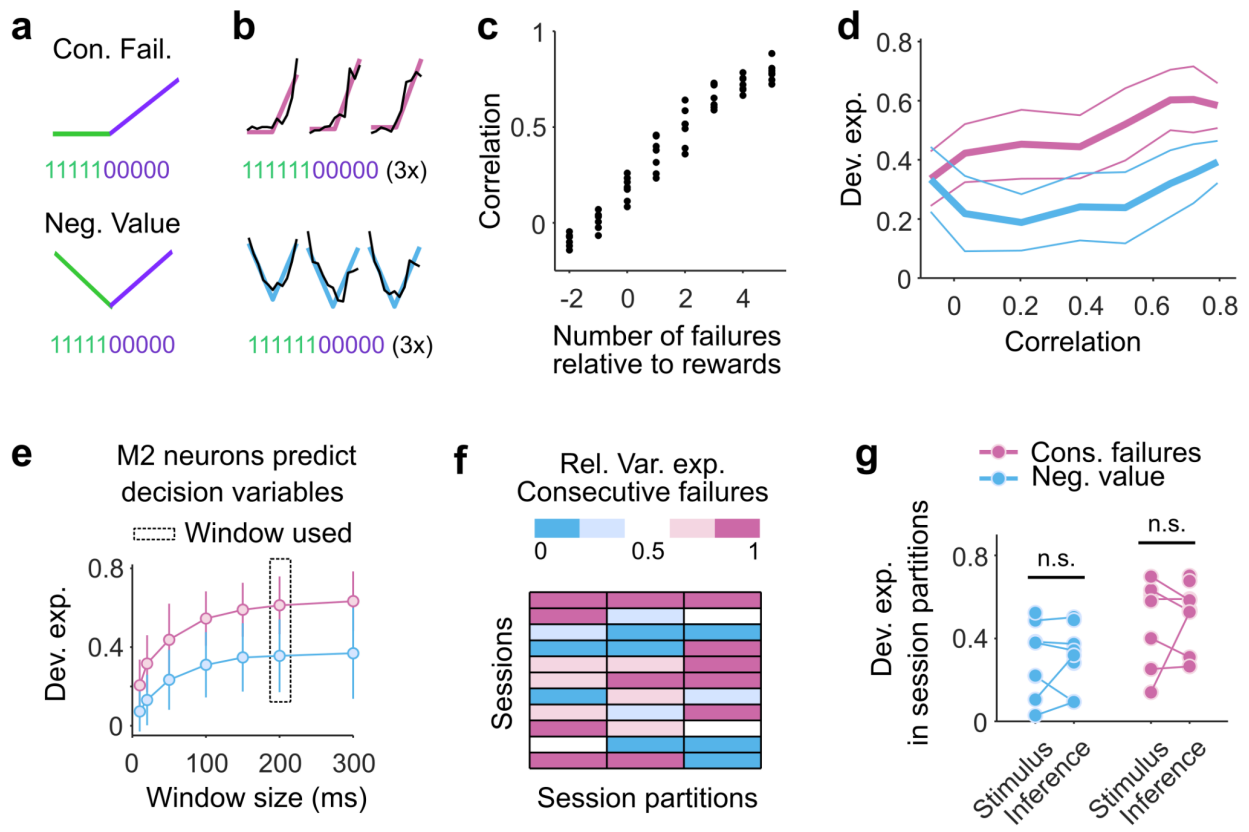

Figure 5: Independent and simultaneous representations of DVs.

(a) Two different sequences relying on different computations involving reset (top) and accumulations (bottom) of rewards.

(b) Three example bouts (columns) of population activity (black traces) projected onto the dimensions that best predict the trajectory of the different sequences (color traces). Only subsequences of consecutive rewards followed by consecutive failures were selected in order to visualize the different computations in (a) (~5% of bouts).

(c) Selecting subsets of action outcomes where the total number of failures changes relative to the number of rewards (abscissa) alter the correlation between sequences generated with the computations in (a) (ordinates). Black dots for each value of the number of failures represents a recording session.

(d) How well the sequences relying on the two different computations can be decoded from M2 (ordinates) as a function of the correlation between them (median ± MAD across sessions). Pink are sequences that accumulate failures and reset with rewards (equivalent to 'consecutive failures'). Blue are sequences that accumulate failures upward and rewards downward (equivalent to 'negative value').

(e) Deviance explained across sessions (median ± MAD) for DVs (color coded as in d) as a function of window sizes. The window used for all other analyses (200 ms) is indicated by the black rectangle.

(f) Relative variance explained of the 'Consecutive failures' for predicting the leaving behavior during partitions of recording sessions predicted using the logistic regression as in Fig. 1j. Larger values of the relative variance explained are colored in pink and indicate the mouse mainly uses the inference-based strategy. Conversely, lower values of the relative variance explained are colored in blue, indicating the mouse mainly uses the stimulus-bound strategy.
(g) Deviance explained from models that fit M2 neurons to the DVs (blue: negative value; pink: consecutive failures) during epochs when the stimulus-bound strategy was dominant compared to epochs when the inference-based strategy was dominant. The dominant strategy was selected as the one with more than 50% of relative variance explained.

M2 does not represent arbitrary sequences

Based on these analyses, M2 appears to multiplex two different DVs that embody stimulus-bound and inference-based strategies, regardless of the extent to which each of these strategies is used by the mouse. This raises the question of whether the DVs available in M2 have any special significance from the point of view of the representational capacity of M2, or whether any time-series containing time-scales roughly matched to the behavioral task can be decoded from M2 neural populations.

Such 'near universal' representational capacity is a feature of a computational framework known as 'reservoir computing'[9,10,12,24] which exploits a potential functional capacity of recurrent networks to represent combinations of current inputs with previous evidence. Recurrent networks are also capable of multiplexing in order to generate non-linear high-dimensional representations[25,26]. To test whether M2 also represented arbitrary signals, we examined whether sequences with similar temporal structure as the DVs but with no obvious relevance to the task could be decoded from M2 (Fig. 6a). For instance, we tested whether M2 neurons represented the DVs but shifted in time (Fig. 6b) or flipped in time across the session (Fig. 6c), and also random signals generated with equal power spectrums as the DVs (Fig. 6d; 100 iterations per session and DVs). We found that shifting the DVs by a delay greater than their temporal autocorrelation greatly impaired their decodability (one-way ANOVA, $F = 62.81$, $p < 10^{-4}$) and that none of the flipped or random signals were decodable from M2 population activity. We also probed the capacity of M2 to represent arbitrary temporal sequences by testing whether we could decode from M2 a basis set of cosine functions with wavelengths in the dynamic range of what we observed with integration and reset of rewards (1 to 4 licks, example on Fig. 6e top), since any signal can be approximated by sums of periodic functions (Fourier analysis). Again, we found that the decoding quality of the periodic function was close to chance level (Fig. 6e; Dev. Exp. = 0.024 ± 0.028, median ± MAD). Together, these series of analyses suggest that M2 does not represent arbitrary temporal sequences.

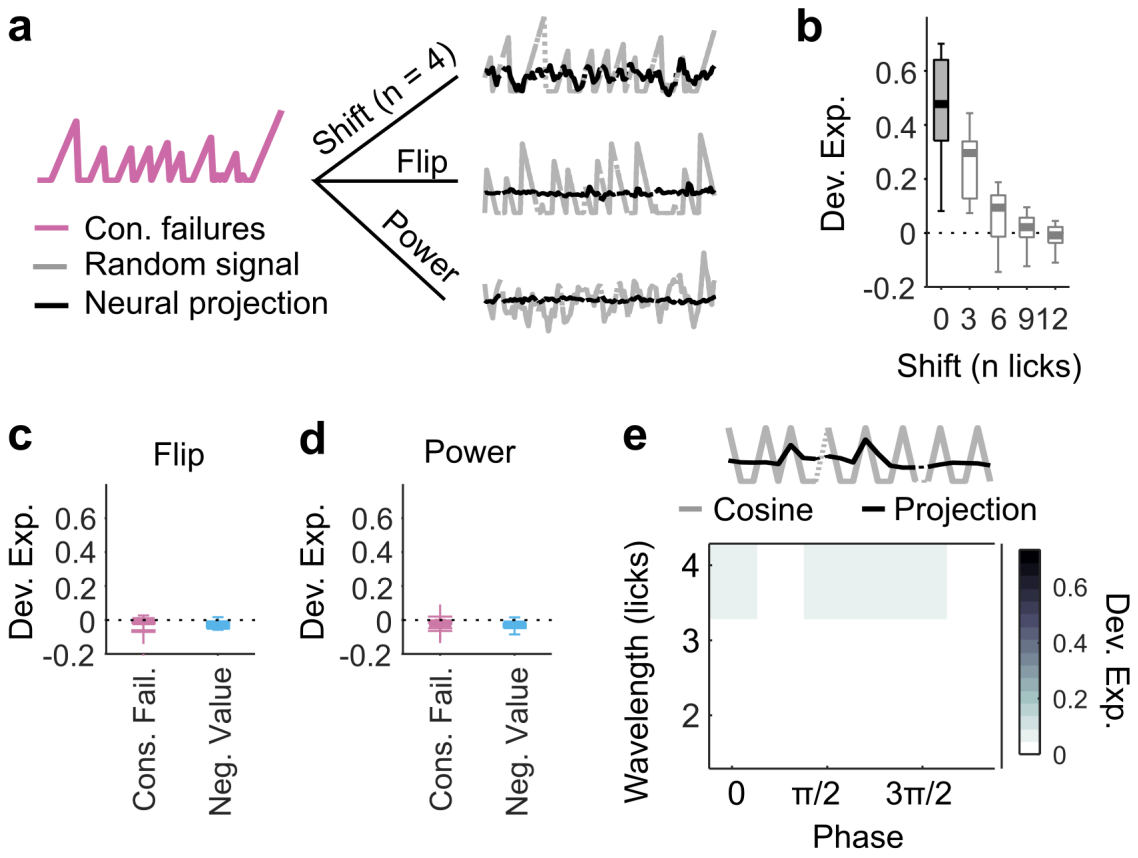

Figure 6: M2 does not represent arbitrary sequences.

(a) Example of random sequences (gray) generated from one of the DVs (pink, here consecutive failures). The DV can lead to a shifted version (top right), a flipped version (middle right) or a random signal with equal power spectra. Each random signal is then decoded from M2 population activity (black traces).

(b) Deviance explained (ordinate) by M2 neurons from decoding the DVs shifted by a given number of licks (abscissa). On each box, the central mark indicates the median across recording sessions, and the bottom and top edges of the box indicate the 25th and 75th percentiles, respectively. The whiskers extend to the most extreme data points. The dash black line indicates chance level (Dev. Exp. = 0).

(c) Same as in (b) but for DVs flipped across sessions.

(d) Same as in (c) but for random signals with power spectra that match each DV.

(e) Decoding periodic sequences generated by cosine functions from M2 population activity. Top: example of cosine signal (gray; wavelength = 4 licks, phase = 0 rad, Dev. Exp. = -0.002) and neural projection (black). Bottom: matrix of deviance explained from decoding sequences with different wavelengths and phases with M2 population activity.

M2 represents foraging algorithms

Since M2 does not encode random combinations of sensory inputs, we next considered that the space of signals encoded in M2 might be restricted to potentially meaningful variables generated from a common set of essential computations. Here, the two DVs we have been considering could both be conceptualized as an adaptive, outcome-dependent feedback gain on a running count. For instance, if we refer to the running count after the *t*-th lick as x_t and to the outcome of the next lick as o_{t+1} (equal 1 or 0 if the outcome is a reward or a failure respectively), then we can write the update rule compactly as

$$x_{t+1} = g(o_{t+1})x_t + c(o_{t+1})$$

with $g(o_{t+1} = 1) = 0$, $g(o_{t+1} = 0) = 1$, and $c(o_{t+1} = 1) = c(o_{t+1} = 0) = 1$ for the inference-based DV, and $g(o_{t+1} = 1) = g(o_{t+1} = 0) = 1$, and $c(o_{t+1} = 0) = -c(o_{t+1} = 1) = 1$, for the stimulus-bound DV. This realization suggests that a common generative model, which we named the FORAging GEnerative model or 'FORAGE model', can produce these two different DVs by adjusting certain model parameters. In the simplest instantiation of this model, the two outcome-dependent parameters are discrete: one is a gain factor (*g*) that specifies whether the running count should be reset or accumulated by each outcome – a non-linear operation – and the other (*c*) specifies how each outcome linearly contributes to the resulting running count, which in general could be positive, negative, or zero (leaving it unaffected; see Methods for more details). Each specification of these two discrete parameters leads to a different DV (Fig. 7a). The FORAGE model thus describes, within a single algorithmic framework, the computations necessary to generate not only the two DVs considered so far, but also other DVs. It is interesting to note that these DVs are actually related to those relevant for a variety of commonly studied behavioral tasks. For instance a 'global count' (accumulated number of outcomes) DV is related to counting or timing tasks[27,28]. Similarly, matching tasks involving randomly timed, cached rewards, are optimally solved by integrating the difference between rewards and failures with an exponential decay[17]. Other integration tasks, like the 'poisson clicks' task require perfect integration of two variables[18]. Thus, the space of DVs generated by the FORAGE model covers a large space of tasks that have been studied in the lab and might be useful in different behavioral contexts.

All non-trivial time series produced by the FORAGE model can be expressed as linear combinations of four basis sequences (Fig. 7a; Methods). The two sequences involving reset describe integration of failures and reset by rewards ('consecutive failures') and vice-versa ('consecutive rewards'). The two sequences for accumulation without reset are upwards integration of both rewards and failures (equivalent to 'count') and integration upwards of

rewards and downwards of failures (equivalent to 'negative value'). We already know that M2 simultaneously represents two of these basis elements ('consecutive failures' and 'negative value'). Thus, we tested whether M2 also represented the two additional basis sequences. We found that, indeed, 'Consecutive reward' and 'Count' could be decoded from the M2 population (Fig. 7b, Wilcoxon signed rank test: $p < 10^{-3}$ for both), and remained decodable from the M2 population when using the subsequences that decorrelate the variables (Fig. 7c; Wilcoxon signed rank test: $p = 0.002$ for 'Consecutive reward' and $p < 10^{-3}$ for 'Count'). In particular, the sequences that consisted of integration of both reward and failures in the same direction ('Count') could be recovered with high accuracy.

Because the individual basis sequences were all relatively well represented in M2, the M2 populations could, in theory, represent each DV that the FORAGE model can produce when fed with the sequences of action outcomes experienced by the mouse. As predicted, this repertoire was indeed decodable from M2 population activity (Fig. 7d).

The FORAGE model can be extended, through analog values of 'g', to produce sub- or supra-linear integration with different time constants. Note that adjusting analog parameter values can directly relate the FORAGE model to frameworks of reinforcement learning with differential learning, where the "reset" is equivalent to a very large negative rate of decay. Therefore, we further tested the richness of the actual FORAGE model family instantiated by M2 by decoding sequences generated with analog 'g' (see example in Fig. 7e). We found that M2 could also represent sublinear integration of rewards and failures, and even supralinear integrations with small time constant ($g(o_{t+1}) < 1.2$, Fig. 7e). Comparing across this parameter space (Fig. 7f), we observed that M2 had a preferred mode of integration that consisted of mostly perfect integration of failures ($0.85 \leq g(o_{t+1} = 0) \leq 1$) and sublinear integration of rewards with a variety of time constants ($g(o_{t+1} = 1) \leq 1$). Altogether, our results show that M2 simultaneously represents a relatively large repertoire of computations that embody a variety of foraging DVs, potentially spanning a set of optimal strategies for environments with different dynamics for the latent state.

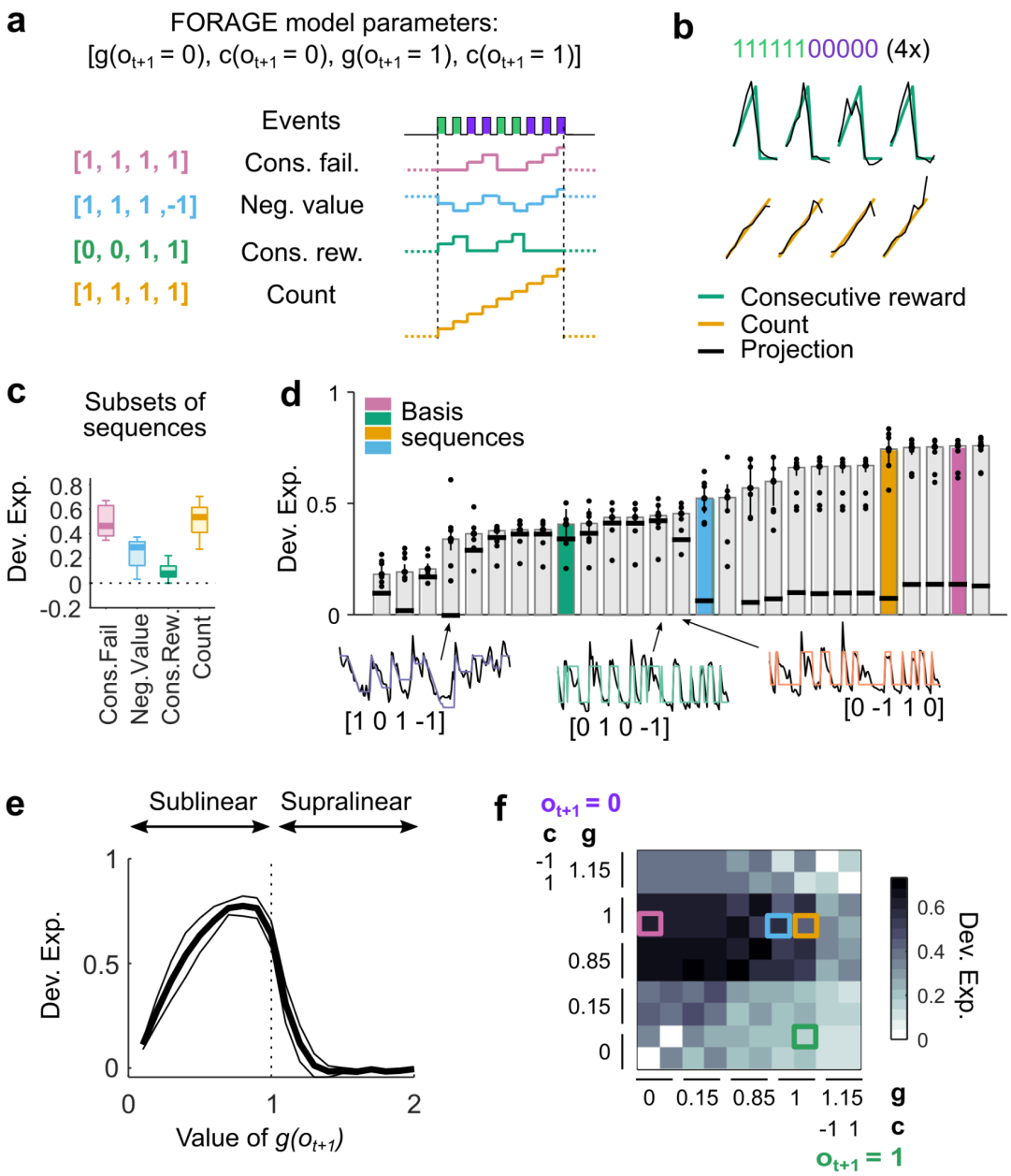

Figure 7: M2 represents foraging algorithms.

(a) The FORAGE model with four parameters generates different time series by accumulating, resetting or ignoring each possible event (reward or failure). Example set of parameters yielding the example DVs on the right.

(b) Four example bouts (columns) of population activity (black traces) projected onto the dimensions that best predict the trajectory of the 'Consecutive rewards' (green) and 'Count' (yellow). Only subsequences of consecutive rewards followed by consecutive failures were selected to highlight the computations underlying the different variables.

(c) Deviance explained across sessions (median ± 25th and 75th percentiles) of the 4 basis sequences decoded from M2 population activity. The sequences were decorrelated using the same method as in Fig. 5c,d.
(d) The decoding quality of each time series generated from the FORAGE model (bar is the median ± MAD of deviance explained across recordings, dots represent single recording sessions), including the basis elements (green, blue, yellow, pink). Black lines indicate the averaged performance estimated from randomly shuffling of rewards and failures to test explicitly the contribution of observable events to these decision representations (100 shuffles per recording of the population activity among time bins for which the outcome of each lick was the same). Example time series from three different classes of computations (i.e., accumulation, reset and outcome; normalized color traces) and the projections of neural activity on the decoding weights for these time series (black traces).
(e) Deviance explained from decoding sublinear and supralinear integrations by M2 population activity. Here, we show an example where the parameters of the FORAGE model are: $c(o_{t+1} = 0) = c(o_{t+1} = 1) = 1$ and $g(o_{t+1} = 0) = g(o_{t+1} = 1)$.
(f) Matrix of deviance explained from decoding sequences with different time constants (corresponding to different values of *g*) of integrations of rewards (columns) and failures (rows) with M2 population activity. The basis sequences are indicated by the color-coded squares.

DISCUSSION

Here, we explored the capacity of several regions of the cortex to deploy different algorithms for generating a diversity of DVs. We studied this in the context of a foraging task whose solution required mice to process streams of successful and unsuccessful foraging attempts (licks) executed over several seconds. We found that mice could use not one but a set of processing strategies to time their decision to leave a foraging site, all of which could be well read out from populations of neurons in M2. Moreover, we found that the set of potentially relevant DVs were actually implemented in parallel within the same neural populations. While 'causal' manipulations of M2 using optogenetic inactivation showed that M2 was important to the deployment of these DVs, we found that the neural availability of alternative DVs was nearly independent of the actual behaviorally-deployed DV. Functionally, the ability of M2 populations to multiplex the computation of several DVs, could allow the mice to rapidly explore and adapt behavior to dynamically changing environmental contingencies by simply modifying linear readouts of M2 neural populations[29,30] without the need to implement new computations.

The different DVs in M2 were "mixed" but could be recovered through linear decoding. Although multiplexed neural codes have been observed previously in other cortical

regions[7,9,25,26,31], our results establish that the kind of information that is multiplexed is not limited to representations of instantaneously observable events in premotor regions, but also includes temporally extended computations spanning several seconds. To some degree, the observation of multiplexed DVs is consistent with the framework of 'reservoir' computing[9,10,12,24]. However, whereas reservoir style computing envisions a pool of random computations, we found that M2 specifically implemented a substantial but specifically circumscribed pool of potentially behaviorally meaningful computations.

The subset of computations available in M2 could be described as the outputs of a generative model of DVs potentially relevant for the task at hand. This model can be considered to be a useful hypothesis concerning a basis set of computations (temporal accumulation and reset) with wide applicability, both within the context of foraging and beyond. As far as we can tell, most tasks concerning the temporal statistics of action outcomes known to have been solved by a mouse, can be efficiently approached within the FORAGE basis.

One computation included in the FORAGE model is accumulation of evidence, which, through its intimate relationship with posterior beliefs[32,33], constitutes an essential computation for statistical inference, and has therefore been implicated in a variety of decision-making and reasoning tasks[18,34–38]. Accumulation (possibly temporally discounted) of action outcomes also underlies several reinforcement learning algorithms[39–42]. Although less attention has been devoted to reset-like computations (but see Ref[43]), they are also essential for inference when certain observations specify a state unambiguously[16].

The two strategies that we describe in the context of foraging represent a particular example of a more general phenomenon. In complex environments, agents can adapt their behavior in different ways depending on how accurately they can infer and specify the relevant causal structure[44], a process which, in the lab, can be described as finding the correct "task representation". Even if unable to apprehend the true causal model, agents can display reasonably well adapted behavior by leveraging the predictive power of salient environmental events. However, because the task representation is not correct, the association between these events and outcomes will necessarily be more probabilistic from the point of view of the agent. Such agents incorrectly model unexplained outcome variance (arising from incomplete task representations) as unexplainable, and often resort to exploratory strategies that are adaptive in what they construe as highly volatile environments[45,46]. Our stimulus-bound strategy is an example of this phenomenon. Lapsing in psychophysical discrimination tasks – i.e, errors that cannot be attributed to sensory limitations[47] – can also be interpreted as exploratory choices that are made when a failure to aprehend the true stimulus dimension that needs to be discriminated is interpreted by the agent as evidence for probabilistic action-outcome mappings[48]. Our results suggest that, at least in the case of foraging, the computations necessary to implement strategies

lying along this continuum are computed simultaneously and available, which might facilitate the process of "insight" necessary to switch between them.

Our finding also speaks to the debate on the nature of serial processing limitations in the brain. While it has been shown that limitations apply in some kinds of evidence accumulation tasks[2,4,49], here we show in a different, but ecologically important, setting that some forms of evidence accumulation can proceed in parallel. An important difference between our task and standard behavioral paradigms that study cognitive bottlenecks is that our mice do not need to simultaneously compute two DVs to perform the task successfully. Nevertheless, we show unambiguously that neural populations in the premotor cortex of mice using a strategy where a single reward resets a counter of failures, reveal both this reset, and simultaneously the updating of a reward counter. Our findings are thus consistent with proposals favoring parallel integration[50–52] and with models that place serial constraints on behavior close to the specification of the timing of action[50,53].

METHODS

Animal subjects

A total of 30 adult male and female mice (24 C57BL/6J and 6 VGAT, 2-9 months old) were used in this study. All experimental procedures were approved and performed in accordance with the Champalimaud Centre for the Unknown Ethics Committee guidelines and by the Portuguese Veterinary General Board (Direco-Geral de Veterinria, approval 0421/000/000/2016). During training and recording, mice were water-restricted (starting 5 to 10 days after head-bar implantation), and sucrose water (10%) was available to them only during the task. Mice were given 1 mL of water or 1 gram of hydrogel (Clear H2O) on days when no training or recording occured or if they did not receive enough water during the task.

Surgery and head-fixation

All surgeries used standard aseptic procedures. Mice were deeply anesthetized with 4% isoflurane (by volume in O_2) and mounted in a stereotaxic apparatus (Kopf Instruments). Mice were kept on a heating pad and their eyes were covered with eye ointment (Vitaminoftalmina A). During the surgery, the anesthesia levels were adjusted between 1% and 2% to achieve 1/second breathing rate. The scalp was shaved and disinfected with 70% ethanol and Betadine. Carprofen (non-steroidal anti-inflammatory and analgesic drug, 5 mg/kg) was injected subcutaneously. A flap of skin (less than $1cm^2$) was removed from the dorsal skull with a single cut and the skull was cleaned and dried with sterile cotton swabs. The bone was scraped with a delicate bone scraper tool and covered with a thin layer of cement (C&B super-bond). Four small craniotomies were drilled (HM1 005 Meisinger tungsten) between Bregma and Lamba (around −0.5 and −1

AP; ±1 ML) and four small screws (Antrin miniature specialities, 000-120x1/16) previously soaked in 90% ethanol, were inserted in the craniotomies in order to stabilize the implant. The head-bar (stainless steel, 19.1 × 3.2 mm), previously soaked in 90% ethanol, was positioned directly on top of the screws. Dental cement (Tab 2000 Kerr) was added to fix the head-bar in position and to form a well around the frontal bone (from the head-bar to the coronal suture). Finally an external ground for electrophysiological recording (a male pin whose one extremity touched the skull) was cemented onto the head-bar.

Behavioral apparatus

Head-fixed mice were placed on a linear treadmill with a 3D printed plastic base and a conveyor belt made of Lego small tread links. The running speed on the treadmill was monitored with a microcontroller (Arduino Mega 2560), which acquired the trace of an analog rotary encoder (MAE3 Absolute Magnetic Kit Encoder) embedded in the treadmill. The treadmill could activate two movable arms via a coupling with two motors (Digital Servo motor Hitec HS-5625-MG). A lick-port, made of a cut and polished 18G needle, was glued at the extremity of each arm. Water flowed to the lick-port by gravity through water tubing and was controlled by calibrated solenoid valves (Lee Company). Licks were detected in real time with a camera (Sony PlayStation 3 Eye Camera or FLIR Chameleon-USB3) located on the side of the treadmill. Using BONSAI[54], an open-source visual programming language, a small squared region of interest was defined around the tongue. To detect the licks a threshold was applied to the signal within the region of interest. The behavioral apparatus was controlled by microcontrollers (Arduino Mega 2560) and scientific boards (Champalimaud Hardware platform), which were responsible for recording the time of the licks and the running speed on the treadmill, and for controlling water-reward delivery and reward-depletion according to the statistics of the task.

Task design

In the foraging task, two reward sites, materialized by two movable arms, could be exploited. Mice licked at a given site to obtain liquid reward and decided when to leave the current site to explore the other one. Each site could be in one of two states: “ACTIVE”, i.e. delivering probabilistic reward, or “INACTIVE”, i.e. not delivering any reward. If one of the sites was “ACTIVE”, the other one was automatically “INACTIVE”. Each lick at the site in the “ACTIVE” state yielded reward with a probability of 90% , and could cause the state to transition to “INACTIVE” with a probability of 30%. Licks could trigger the state of the exploited site to transition from “ACTIVE” to “INACTIVE”, but never the other way around. Importantly, this transition was hidden to the animal. Therefore, mice had to infer the hidden state of the exploited site from the history of rewarded and unrewarded licks (i.e., reward and failures). We defined ‘behavioral bout’ the sequence of consecutive licks at one spout. A tone (150 ms, 10 kHz) was played when one of the arms moved into place (i.e., in front of the mouse) to signal that a bout could start. At the tone, the closed-loop between the motors and the

treadmill decoupled during 1.5 s or until the first valid lick was detected. During this time mice had to "STOP", i.e. decrease their running speed for more than 250 ms below a threshold for movement (3 cm/s). Licks were considered invalid if they happened before "STOP" or at any moment after "STOP" if the speed was above the threshold. If a mouse failed to "STOP", "LEAVE" was triggered by reactivating the closed-loop after 1.5 s, which activated the movement of the arms (the one in front moved away and the other moved into place). Mice typically took around 200 ms to "STOP" and initiate valid licking. During the licking periods, each lick was rewarded in a probabilistic fashion by a small drop of water (1 µl). The small reward size ensured that there was no strong difference in licking rate between rewarded and unrewarded licks. To "LEAVE", mice had to restart running above the threshold for movement for more than 150 ms, and travel a fixed distance on the treadmill (around 16 cm) to reach the other arm. We defined as correct bouts the ones in which mice stopped licking after the states transitioned from "ACTIVE" to "INACTIVE". Error bouts were ones in which mice stopped licking before the state transition occurred. In this case, mice had to travel double the distance to get back to the arm in "ACTIVE" state. Missed bouts were ones in which mice alternated between arms without any valid lick. These 'missed bouts' were excluded from our analysis.

Mouse training

Mice were handled by the experimenter from 3 to 7 days, starting from the beginning of the water restriction and prior to the first training session. At the beginning of the training, mice were acclimatized to the head-fixation and to the arm movement and received liquid reward simply by licking at the lick-port. The position of the lick-ports relative to the snout of the mouse had an important effect on behavioral performances. Thus, to ensure that the position of the lick-ports remained unchanged across experimental sessions, it was carefully adjusted on the first session and calibrated before the beginning of every other session. After mice learned to lick for water reward (typically after one or two sessions), the next sessions consisted of an easier version of the task (with low probability of state transition, typically 5% or 10%, and high probability of reward delivery, 90%), and both arms in "ACTIVE" state. That way, if mice alternated between arms before the states of the sites transitioned, the other arm would still deliver reward and animals would not receive the travel penalty. Occasionally during the early phase of training, manual water delivery was necessary to motivate the mice to lick or to stop running. Alternatively, it was sometimes necessary to gently touch the tail of the animals, such that they started to run and gradually associated running with the movement of the arms. The difficulty of the following sessions was progressively increased by increasing the probability of state transition if the performance improved. Performance improvement was indicated by an increase in the number of bouts and licking rate, and by a decrease in the average time of different events within a bout. Mice were then trained for at least five consecutive days on the final task before the recording sessions.

Electrophysiology

Recordings were made using electrode arrays with 374 recording sites (Neuropixels "Phase3A"). The Neuropixels probes were mounted on a custom 3D-printed piece attached to a stereotaxic apparatus (Kopf Instruments). Before each recording session, the shank of the probe was stained with red-fluorescent dye (DiI, ThermoFisher Vybrant V22885) to allow later track localization. Mice were habituated to the recording setup for a few days prior to the first recording session. Prior to the first recording session, mice were briefly anesthetized with isoflurane and administered a non-steroidal analgesic (Carprofen) before drilling one small craniotomy (1 mm diameter) over the secondary motor cortex. The craniotomy was cleaned with a sterile solution and covered with silicone sealant (Kwik-Sil, World Precision Instruments). Mice were allowed to recover in their home cages for several hours before the recording. After head-fixation, the silicone sealant was removed and the shank of the probe was advanced through the dura and slowly lowered to its final position. The craniotomies and the ground-pin were covered with a sterile cortex buffer. The probe was allowed to settle for 10 min to 20 min before starting recording. Recordings were acquired with SpikeGLX Neural recording system (https://billkarsh.github.io/SpikeGLX/) using the external reference setting and a gain of 500 for the AP band (300 Hz high-pass filter). Recordings were made from either hemisphere. The target location of the probe corresponded to the coordinates of the anterior lateral motor cortex, a region of the secondary motor cortex important for motor planning of licking behavior[21]. The probe simultaneously traversed the orbitofrontal cortex, directly ventral to the secondary motor cortex. In a subset of recording sessions (9 out of 11), a large portion of the probe tip ended in the olfactory cortex, ventral to the orbitofrontal cortex.

Histology and probe localization

After the recording session, mice were deeply anesthetized with Ketamine/Xylazine and perfused with 4% paraformaldehyde. The brain was extracted and fixed for 24 hours in paraformaldehyde at 4 C, and then washed with 1% phosphate-buffered saline. The brain was sectioned at 50 µm, mounted on glass slides, and stained with 4',6-diamidino-2-phenylindole (DAPI). Images were taken at 5x magnifications for each section using a Zeiss AxioImager at two different wavelengths (one for DAPI and one for DiI). To determine the trajectory of the probe and approximate the location of the recording sites, we used SHARP-Track [55], an open-source tool for analyzing electrode tracks from slice histology. First, an initial visual guess was made to find the coordinates from the Allen Mouse Brain Atlas (3D Allen CCF, http://download.alleninstitute.org/informatics-archive/current-release/mouse_ccf/annotation/) for each DiI mark along the track by comparing structural aspects of the histological slice with features in the atlas. Once the coordinates were identified, slice images were registered to the atlas using manual input and a line was fitted to the DiI track 3D coordinates. As a result, the atlas labels along the probe track were extracted and aligned to the recording sites based on their location on the shank. Finally, we also used characteristic physiological features to refine the

alignment procedure (i.e, clusters of similar spike amplitude across cortical layers, low spike rate between frontal and olfactory cortical boundaries, or LFP signatures in deep olfactory areas).

Optogenetic stimulation

To optically stimulate ChR2 expressing VGAT-expressing GABAergic interneurons we used blue light from a 473 nm laser (LRS-0473-PFF-00800-03, Laserglow Technologies, Toronto, Canada, or DHOM-M-473-200, UltraLasers, Inc., Newmarket, Canada). Light was emitted from the laser through an optical fiber patch-cord (200 µm, 0.22 NA, Doric lenses), connected to a second fiber patch-cord with a rotatory joint (FRJ 1x1, Doric lenses), which in turn was connected to the chronically implanted optic fiber cannulas (M3 connector, Doric lenses). The cannulas were inserted bilaterally inside small craniotomies performed on top of M2 (+2.5 mm anterior and ±1.5mm lateral of bregma) and barely touched the dura (as to avoid damaging superficial cortical layers). Structural glue (Super-bond C&B kit) was used to fix the fiber to the skull. The power of the laser was calibrated before every session using an optical power meter kit (Digital Console with Slim Photodiode Sensor, PM100D, Thorlabs). During the foraging task, the optical stimulation (10 ms pulses, 75 s^{-1}, 5 mW) was turned on during 30% of randomly interleaved bouts. Light delivery started when the first lick was detected and was interrupted if the animal did not lick for 500 ms (which was in 98% of bouts after the last lick of the bouts).

Pre-processing neural data

Neural data were pre-processed as described previously[56]. Briefly, the neural data were first automatically spike-sorted with Kilosort2 (https://github.com/MouseLand/Kilosort) using MATLAB (MathWork, Natick, MA, USA). To remove the baseline offset of the extracellular voltage traces, the median activity of each channel was subtracted. Then, to remove artifacts, traces were "common-average referenced" by subtracting the median activity across all channels at each time point. Second, the data was manually curated using an open source neurophysiological data analysis package (Phy: https://github.com/kwikteam/phy). This step consisted in categorizing each cluster of events detected by a particular Kilosort template into a good unit or an artifact. There were several criteria to judge a cluster as noise (non-physiological waveform shape or pattern of activity across channels, spikes with inconsistent waveform shapes within the same cluster, very low-amplitude spikes, and high contamination of the refractory period). Units labeled as artifacts were discarded in further analyses. Additionally, each unit was compared to spatially neighboring units with similar waveforms to determine whether they should be merged, based on cross-correlogram features and/or drift patterns. Units passing all these criteria were labeled as good and considered to reflect the spiking activity of a single neuron. For all analyses, otherwise noted, we averaged for each neuron the number of spikes into bins by considering a 200 ms window centered around each lick. The bin-vectors were then z-scored. Because the interval between each lick was on average around 150 ms, there was little

overlap between two consecutive bins and each bin typically contained the number of spikes associated with only one lick.

Predicting choice from DVs

All data analyses were performed with custom-written software using MATLAB. We used logistic regression[57] to estimate how DVs predicted the choice of the animal (i.e., the probability that the current lick is the last in the bout). Using Glmnet for Matlab (Qian, J., Hastie, T., Friedman, J., Tibshirani, R. and Simon, N., 2013; http://www.stanford.edu/~hastie/glmnet_matlab/) with binomial distribution, model fits were performed with DVs as predictors. We used 5-fold nested cross-validation and elastic net regularization (α = 0.5). To assess a metric of model fit, we calculated the deviance explained (as implemented by the devianceTest function in Matlab). The deviance explained is a global measure of fit that is a generalization of the determination coefficient (r-squared) for generalized linear models. It is calculated as:

$$Deviance\ explained\ = 1 - \frac{residual\ deviance}{null\ deviance}.$$

The residual deviance is defined as twice the difference between the log-likelihoods of the perfect fit (i.e., the saturated model) and the fitted model. The null deviance is the residual deviance of the worst fit (i.e the model that only contains an intercept). The log-likelihood of the fitted model is always smaller than the log-likelihood of the saturated model, and always larger than the log-likelihood of the null model. As a consequence, if the fitted model does better than the null model at predicting choice, the resulting deviance explained should be between 0 and 1. When the fitted model does not predict much better than the null model, the deviance explained is close to zero.

Simulated behavior sessions

To test the logistic regression model, we simulated behavioral sessions of an agent making decisions using a logistic function and the DV of the inference strategy (consecutive failures). For each simulated session, the slope and the intercept of the logistic regression in the ground truth model were chosen to fit the distribution of the total number of licks in each bout from the real data. To estimate the parameters of the ground truth model (slope and intercept), we then fit a logistic regression model to predict the leaving decisions of this simulated agent using the consecutive failures DVs.

Predicting DVs from neural population

We used a generalized linear regression model for Poisson response [58] to predict each DV given the activity of the neural population (or facial motion, or both). Specifically, we predicted the DV

A given the neural activity x, by learning a model with parameters, β, such as $A = exp(\beta_0 + \beta x)$. The Poisson regression with log-link is appropriate to model count data like the DVs studied here. To enforce positivity of the count responses, we shifted all the DVs to have a minimum value of one. Model fits were performed on each session separately. We employed elastic net regularization with parameter $\alpha = 0.5$. Additionally, we performed a cross-validation implemented by cvglmnet using the lambda_min option to select the hyper-parameter that minimizes prediction error. To assess the predictive power of the model, we also implemented a nested cross-validation. Specifically, the model coefficients and hyperparameters were sequentially fit using a training set consisting of four-fifths of the data and the prediction was evaluated on the testing set consisting of the remaining one-fifth. The method was implemented until all the data had been used both for training and testing. The deviance explained reported as a metric of the goodness of fit was calculated from the cross-validated results. The final β coefficients were estimated using the full dataset.

Comparison between brain regions

To ensure fair comparison between brain regions with different numbers of recorded neurons, we excluded regions with very low numbers of recorded neurons (i.e. less than 20 neurons, n = 2 recordings in Olf excluded) and used multiple approaches to match the data from each region. One approach was to run principal component analysis of the neural data from each region and select the principal components of neural activity that predicted up to 95% of the total variance (as reported in Fig. 2). A second approach was to select a subset of the original data to match the lowest number of neurons per region in each recording (subsampling with replacement, 100 repetitions). Both approaches yielded qualitatively similar results.

Predicting choice from neural population

We used logistic regression[57] to estimate how the weighted sum of neural activity (i.e., the neural projections onto the weights that best predict the various DVs) predicted the probability that the current lick is the last in the bout. The model fit each recording session separately as described above using the glmnet package in MATLAB and implementing elastic net regularization with $\alpha = 0.5$ and a nested 5-fold cross validation to estimate the deviance explained.

Model

We developed a unified theory of integration in the setting of non-sensory decision making tasks. In a wide variety of tasks, animals need to keep track of quickly evolving external quantities. Here, we considered tasks where the feedback that the animal receives is binary (e.g. reward or failure). We considered an integrator given by $x_{t+1} = g(o_{t+1} = 1) \bullet x_t + c(o_{t+1} = 1)$, if the attempt is rewarded, and $x_{t+1} = g(o_{t+1} = 0) \bullet x_t + c(o_{t+1} = 0)$, otherwise. The parameters of the integrator $g(o_{t+1} = 0)$ and $g(o_{t+1} = 1)$ represent the computations and are bound between zero and one (g = 1

for an accumulation, g = 0 for a reset). The parameters $c(o_{t+1} = 1)$, $c(o_{t+1} = 0)$ add linearly and can be negative, positive or null.

We consider different scenarios involving a combination of computations but where the optimal solution only involves a one-dimensional integration. For instance, counting tasks can be solved by a linear integration, i.e. $g(o_{t+1} = 0) = g(o_{t+1} = 1) = c(o_{t+1} = 0) = c(o_{t+1} = 1) = 1$, where the integrated value increases by one after each attempt regardless of the outcome. In a two-alternative forced choice and more generally in an n-armed bandit task, each arm would have an integrator that increases with rewards i.e, $g(o_{t+1} = 0) = g(o_{t+1} = 1) = 1$, $c(o_{t+1} = 0) = 0$ and $c(o_{t+1} = 1) = 1$, and decays with failures, i.e., $g(o_{t+1} = 0) = g(o_{t+1} = 1) = 1$, $c(o_{t+1} = 0) = -1$ and $c(o_{t+1} = 1) = 0$. Even in cognitively more complex tasks, involving inference over hidden states, such as reversal tasks or foraging under uncertainty, a single integrator is often sufficient. Specifically in the foraging task studied here, the optimal solution is to integrate failures but not rewards, i.e., $g(o_{t+1} = 0) = c(o_{t+1} = 0) = 1$, and $g(o_{t+1} = 1) = c(o_{t+1} = 1) = 0$.

More generally, the model produces sequences that ramp-up with failures (i.e., $g(o_{t+1} = 0) = c(o_{t+1} = 0) = 1$; such as the consecutive failures), and the mirror images that ramp down (i.e., $g(o_{t+1} = 0) = 1$, $c(o_{t+1} = 0) = -1$). Similarly, the model can produce sequences that ramp-up or down with rewards (i.e., $g(o_{t+1} = 1) = 1$, $c(o_{t+1} = 1) = \pm 1$). The model also generates sequences that accumulate one type of event and persist at a constant level with the other type (i.e., $g(o_{t+1} = x) = 1$, $c(o_{t+1} = x) = \pm 1$, $g(o_{t+1} = y) = 1$, $c(o_{t+1} = y) = 0$), such as the cumulative reward integrator or its mirror image. Finally, many sequences generated by the model (where $g(o_{t+1} = 0) = g(o_{t+1} = 1) = 0$) track the outcomes (i.e., reward vs failure).

There are 36 different values that the parameters of the model can take ($g(o_{t+1} = 0)$ and $g(o_{t+1} = 1)$ could take the values of 0 or 1 and $c(o_{t+1} = 0)$ and $c(o_{t+1} = 1)$ could take the values of -1, 0 or 1). In principle, each of these defines a different model which generates a time-series when fed with sequences of binary action outcomes. The 8 of them for which $c(o_{t+1} = 0) = c(o_{t+1} = 1) = 0$ are trivial (constant). Of the remaining 28, not all are linearly independent. For instance, the time series generated by the model that computes 'count' ($g(o_{t+1} = 0) = g(o_{t+1} = 1) = c(o_{t+1} = 0) = c(o_{t+1} = 1) = 1$) is equal to the sum of the time series generated by the model that accumulates reward and is insensitive to failures ($g(o_{t+1} = 0) = g(o_{t+1} = 1) = 1$; $c(o_{t+1} = 0) = 0$; $c(o_{t+1} = 1) = 1$) and the time series generated by the model that accumulates failures and is insensitive to rewards ($g(o_{t+1} = 0) = g(o_{t+1} = 1) = 1$; $c(o_{t+1} = 0) = 1$; $c(o_{t+1} = 1) = 0$). Thus, the rank of the space of time series is 8 (two dimensions for the linear component (*c*) of the model for each of the four possible combinations of the *g* parameters, which specify the 'computation' the model is performing). Out of these 8 dimensions, 4 come from models that are less interesting. Two of these are the two 'outcome' time series ($g(o_{t+1} = 0) = g(o_{t+1} = 1) = 0$), which are 'observable'. We also only consider one time series for each of the two integrate-and-reset models, since the value of the linear component associated with the outcome that is reset makes very little difference to the overall shape of the time series. For instance, the time series generated by the two models $g(o_{t+1} = 0) = 1$; $g(o_{t+1} = 1) = 0$; $c(o_{t+1} = 0) = 1$; $c(o_{t+1} = 1) = 0$ and $g(o_{t+1} = 0) = 1$;

$g(o_{t+1} = 1) = 0$; $c(o_{t+1} = 0) = 1$; $c(o_{t+1} = 1) = 1$ are linearly independent but almost identical for the type of outcome sequences of interest. The remaining 4 dimensions after these 'trival' models are removed are spanned by the 4 basis elements that we focus on in the main text (Fig. 7). Finally, the effective dimensionality of the space of time series also depends on the temporal statistics of the outcome sequences. For the particular outcome sequences experienced by the mice (which are a function of the reward and state-transition probabilities) the effective dimensionality was low, which motivated us to focus on particular subsets of outcome sequences in Fig. 7 where the time series generated by the 4 basis elements are clearly distinct.

RESOURCE AVAILABILITY

Data Availability

The data that support the findings of this study are deposited to Mendeley and available at: LINK.

Data and Code Availability

All analyses were performed using custom code written in MATLAB and available upon request.

ACKNOWLEDGEMENTS

We thank Pietro Vertechi for insightful discussions about the project and the model, Davide Reato for support with analyses, and Luca Mazzucato for comments on the manuscript. We also thank Michael Beckert for assistance with the illustrations. This work was supported by an EMBO long-term fellowship (F.C.; ALTF 461-2016) an AXA postdoctoral fellowship (F.C.), the MEXT Grant-in-Aid for Scientific Research (19H05208, 19H05310, 19K06882, M.M.), the Takeda Science Foundation (M.M.), Fundação para a Ciência e a Tecnologia (PTDC/MED_NEU/32068/2017, M.M., Z.F.M.; and LISBOA-01-0145-FEDER-032077, A.R.), the European Research Council Advanced Grant (671251, Z.F.M.), Simons Foundation (SCGB 543011, Z.F.M.), and Champalimaud Foundation (Z.F.M., A.R.). This work was also supported by Portuguese national funds, through FCT - Fundação para a Ciência e a Tecnologia - in the context of the project UIDB/04443/2020 and by the research infrastructure CONGENTO, co-financed by Lisboa Regional Operational Programme (Lisboa2020), under the PORTUGAL 2020 Partnership Agreement, through the European Regional Development Fund (ERDF) and Fundação para a Ciência e Tecnologia (Portugal) under the projects LISBOA-01-0145-FEDER-02217 and LISBOA-01-0145-FEDER-022122.

AUTHOR CONTRIBUTIONS

F.C. and Z.F.M. conceived the project. F.C. and M.M. designed and performed behavioral experiments. J.P.M. helped with surgery and behavioral training. F.C. designed and performed electrophysiological experiments. F.C. curated the data. F.C. and A.R. designed and performed the analyses. F.C., A.R and Z.F.M. wrote the manuscript. All authors reviewed the manuscript.

DECLARATION OF INTERESTS

The authors declare no competing interests.

REFERENCES

1. Niv, Y. Learning task-state representations. Nat. Neurosci. **22**, 1544–1553 (2019).

2. Kang, Y. H. et al. Multiple decisions about one object involve parallel sensory acquisition but time-multiplexed evidence incorporation. eLife **10**, e63721 (2021).

3. Pashler, H. Processing stages in overlapping tasks: Evidence for a central bottleneck. J. Exp. Psychol. Hum. Percept. Perform. **10**, 358–377 (1984).

4. Sigman, M. & Dehaene, S. Parsing a Cognitive Task: A Characterization of the Mind's Bottleneck. PLOS Biol. **3**, e37 (2005).

5. Scott, B. B. et al. Fronto-parietal Cortical Circuits Encode Accumulated Evidence with a Diversity of Timescales. Neuron **95**, 385-398.e5 (2017).

6. Bernacchia, A., Seo, H., Lee, D. & Wang, X.-J. A reservoir of time constants for memory traces in cortical neurons. Nat. Neurosci. **14**, 366–372 (2011).

7. Mante, V., Sussillo, D., Shenoy, K. V. & Newsome, W. T. Context-dependent computation by recurrent dynamics in prefrontal cortex. Nature **503**, 78–84 (2013).

8. Sussillo, D., Churchland, M. M., Kaufman, M. T. & Shenoy, K. V. A neural network that finds a naturalistic solution for the production of muscle activity. Nat. Neurosci. **18**, 1025–1033 (2015).

9. Enel, P., Procyk, E., Quilodran, R. & Dominey, P. F. Reservoir Computing Properties of Neural Dynamics in Prefrontal Cortex. PLOS Comput. Biol. **12**, e1004967 (2016).

10. Jaeger, H. & Haas, H. Harnessing Nonlinearity: Predicting Chaotic Systems and Saving Energy in Wireless Communication. Science **304**, 78–80 (2004).

11. Laje, R. & Buonomano, D. V. Robust timing and motor patterns by taming chaos in recurrent neural networks. Nat. Neurosci. **16**, 925–933 (2013).

12. Sussillo, D. & Abbott, L. F. Generating coherent patterns of activity from chaotic neural networks. Neuron **63**, 544–557 (2009).

13. Vaswani, A. et al. Attention Is All You Need. ArXiv170603762 Cs (2017).

14. Whittington, J. C. R., Warren, J. & Behrens, T. E. J. Relating transformers to models and neural representations of the hippocampal formation. ArXiv211204035 Cs Q-Bio (2021).

15. Cazettes, F., Reato, D., Morais, J. P., Renart, A. & Mainen, Z. F. Phasic Activation of Dorsal Raphe Serotonergic Neurons Increases Pupil Size. Curr. Biol. CB **31**, 192-197.e4 (2021).

16. Vertechi, P. et al. Inference-Based Decisions in a Hidden State Foraging Task: Differential Contributions of Prefrontal Cortical Areas. Neuron **106**, 166-176.e6 (2020).

17. Sugrue, L. P., Corrado, G. S. & Newsome, W. T. Matching behavior and the representation of value in the parietal cortex. Science **304**, 1782–1787 (2004).

18. Brunton, B. W., Botvinick, M. M. & Brody, C. D. Rats and humans can optimally accumulate evidence for decision-making. Science **340**, 95–98 (2013).

19. Jun, J. J. et al. Fully Integrated Silicon Probes for High-Density Recording of Neural Activity. Nature **551**, 232–236 (2017).

20. Murakami, M., Vicente, M. I., Costa, G. M. & Mainen, Z. F. Neural antecedents of self-initiated actions in secondary motor cortex. Nat. Neurosci. **17**, 1574 (2014).

21. Li, N., Chen, T.-W., Guo, Z. V., Gerfen, C. R. & Svoboda, K. A motor cortex circuit for motor planning and movement. Nature **519**, 51–56 (2015).

22. Green, D. M. & Swets, J. A. Signal detection theory and psychophysics. (New York : Wiley, 1966).

23. Feierstein, C. E., Quirk, M. C., Uchida, N., Sosulski, D. L. & Mainen, Z. F. Representation of Spatial Goals in Rat Orbitofrontal Cortex. Neuron **51**, 495–507 (2006).

24. Tanaka, G. et al. Recent advances in physical reservoir computing: A review. Neural Netw. **115**, 100–123 (2019).

25. Raposo, D., Kaufman, M. T. & Churchland, A. K. A category-free neural population supports evolving demands during decision-making. Nat. Neurosci. **17**, 1784–1792 (2014).

26. Rigotti, M. et al. The importance of mixed selectivity in complex cognitive tasks. Nature **497**, 585–590 (2013).

27. Mello, G. B. M., Soares, S. & Paton, J. J. A Scalable Population Code for Time in the Striatum. Curr. Biol. **25**, 1113–1122 (2015).

28. Simen, P., Balci, F., deSouza, L., Cohen, J. D. & Holmes, P. A Model of Interval Timing by Neural Integration. J. Neurosci. **31**, 9238–9253 (2011).

29. Xiong, Q., Znamenskiy, P. & Zador, A. M. Selective corticostriatal plasticity during acquisition of an auditory discrimination task. Nature **521**, 348–351 (2015).

30. Drugowitsch, J., Mendonça, A. G., Mainen, Z. F. & Pouget, A. Learning optimal decisions with confidence. Proc. Natl. Acad. Sci. **116**, 24872–24880 (2019).

31. Kobak, D. et al. Demixed principal component analysis of neural population data. eLife **5**, e10989 (2016).

32. Wald, A. Sequential Analysis. (John Wiley & Sons, New York., 1947).

33. Drugowitsch, J., Moreno-Bote, R., Churchland, A. K., Shadlen, M. N. & Pouget, A. The

Cost of Accumulating Evidence in Perceptual Decision Making. J. Neurosci. **32**, 3612–3628 (2012).

34. Gold, J. I. & Shadlen, M. N. Banburismus and the Brain: Decoding the Relationship between Sensory Stimuli, Decisions, and Reward. Neuron **36**, 299–308 (2002).

35. Glaze, C. M., Kable, J. W. & Gold, J. I. Normative evidence accumulation in unpredictable environments. eLife **4**, e08825 (2015).

36. Krajbich, I. & Rangel, A. Multialternative drift-diffusion model predicts the relationship between visual fixations and choice in value-based decisions. Proc. Natl. Acad. Sci. **108**, 13852–13857 (2011).

37. Yang, T. & Shadlen, M. N. Probabilistic reasoning by neurons. Nature **447**, 1075–1080 (2007).

38. Sarafyazd, M. & Jazayeri, M. Hierarchical reasoning by neural circuits in the frontal cortex. Science **364**, (2019).

39. Sutton, R. S. & Barto, A. G. Reinforcement learning: an introduction. (MIT Press, 1998).

40. Kaelbling, L. P., Littman, M. L. & Cassandra, A. R. Planning and acting in partially observable stochastic domains. Artif. Intell. **101**, 99–134 (1998).

41. Rao, R. P. N. Decision Making Under Uncertainty: A Neural Model Based on Partially Observable Markov Decision Processes. Front. Comput. Neurosci. **4**, (2010).

42. Rushworth, M. F. S. & Behrens, T. E. J. Choice, uncertainty and value in prefrontal and cingulate cortex. Nat. Neurosci. **11**, 389–397 (2008).

43. Hermoso-Mendizabal, A. et al. Response outcomes gate the impact of expectations on perceptual decisions. Nat. Commun. **11**, 1057 (2020).

44. Gershman, S. J. & Niv, Y. Learning latent structure: Carving nature at its joints. Curr. Opin. Neurobiol. **20**, 251–256 (2010).

45. Thompson, W. R. On the Likelihood that One Unknown Probability Exceeds Another in View of the Evidence of Two Samples. Biometrika **25**, 285–294 (1933).

46. Wilson, R. C., Takahashi, Y. K., Schoenbaum, G. & Niv, Y. Orbitofrontal cortex as a cognitive map of task space. Neuron **81**, 267–279 (2014).

47. Wichmann, F. A. & Hill, N. J. The psychometric function: I. Fitting, sampling, and goodness of fit. Percept. Psychophys. **63**, 1293–1313 (2001).

48. Pisupati, S., Chartarifsky-Lynn, L., Khanal, A. & Churchland, A. K. Lapses in perceptual decisions reflect exploration. eLife **10**, e55490 (2021).

49. Zylberberg, A., Ouellette, B., Sigman, M. & Roelfsema, P. R. Decision Making during the

Psychological Refractory Period. Curr. Biol. **22**, 1795–1799 (2012).

50. Cisek, P. Cortical mechanisms of action selection: the affordance competition hypothesis. Philos. Trans. R. Soc. B Biol. Sci. **362**, 1585–1599 (2007).

51. Gallivan, J. P., Logan, L., Wolpert, D. M. & Flanagan, J. R. Parallel specification of competing sensorimotor control policies for alternative action options. Nat. Neurosci. **19**, 320–326 (2016).

52. Shenhav, A., Straccia, M. A., Musslick, S., Cohen, J. D. & Botvinick, M. M. Dissociable neural mechanisms track evidence accumulation for selection of attention versus action. Nat. Commun. **9**, 2485 (2018).

53. Klapp, S. T., Maslovat, D. & Jagacinski, R. J. The bottleneck of the psychological refractory period effect involves timing of response initiation rather than response selection. Psychon. Bull. Rev. **26**, 29–47 (2019).

54. Lopes, G. et al. Bonsai: an event-based framework for processing and controlling data streams. Front. Neuroinformatics **9**, (2015).

55. Shamash, P., Carandini, M., Harris, K. & Steinmetz, N. A tool for analyzing electrode tracks from slice histology. bioRxiv 447995 (2018) doi:10.1101/447995.

56. Steinmetz, N. A., Zatka-Haas, P., Carandini, M. & Harris, K. D. Distributed coding of choice, action, and engagement across the mouse brain. Nature **576**, 266–273 (2019).

57. Simon, N., Friedman, J. H., Hastie, T. & Tibshirani, R. Regularization Paths for Cox's Proportional Hazards Model via Coordinate Descent. J. Stat. Softw. **39**, 1–13 (2011).

58. Friedman, J. H., Hastie, T. & Tibshirani, R. Regularization Paths for Generalized Linear Models via Coordinate Descent. J. Stat. Softw. **33**, 1–22 (2010).

SUPPLEMENTARY INFORMATION

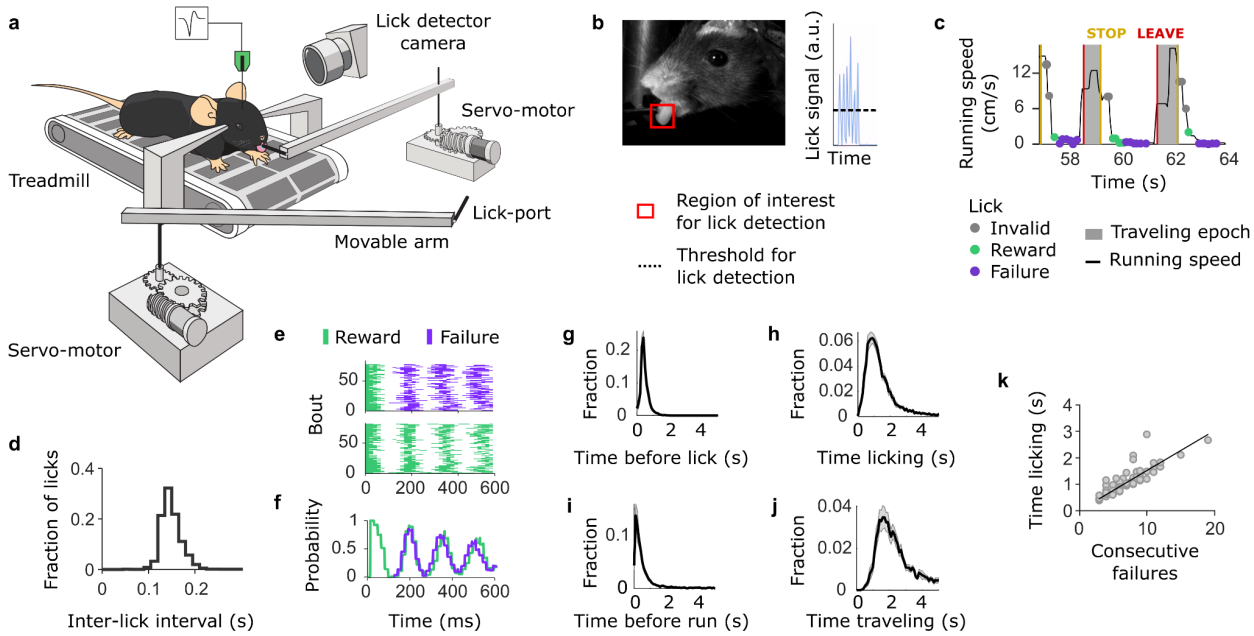

Supplementary Figure 1: Task apparatus and behavioral properties.
(a) The behavioral apparatus consists of a treadmill, coupled to two servo motors. Rotating the treadmill activates in a closed-loop fashion the movement of the arms via the motors. A mouse placed on the treadmill with its head fixed can lick at the spout from the arm in front. A camera placed on the side of the animal allows on-line video detection of the licks.
(b) View from the lick detector camera. A region of interest is defined around the tongue of the animal. To detect the licks a threshold is applied to the signal within the region of interest.
(c) The task consists of behavioral bouts and traveling epochs. Within a behavioral bout, the outcomes of the licks are classified into three types: reward, failure and invalid. Rewards and failures occur when the mouse slows down its running speed below an arbitrary threshold after the 'STOP event'. The 'STOP event' is signaled by an auditory tone when an arm comes into place. Any lick above the running threshold is considered as invalid and always unrewarded. The traveling epoch starts after the 'LEAVE event', when the mouse initiates the run. (d, e, f) The licking behavior of the animals is stereotyped.
(d) Histogram of the time between each lick.
(e) Examples of lick raster of consecutive failures (top) and consecutive rewards (bottom). Licks are aligned at the onset of a rewarded lick and sorted based on the following events.
(f) The licking frequency that corresponds to the two different examples in (e) (series of consecutive rewards in green and series of consecutive failures in purple).

(g, h, i, j) Time distributions of different behavioral events (mean ± s.e.m.; n = 21 mice). The time spent licking was much greater than the time to initiate licking (between STOP event and first lick) or the time to initiate running (between the last lick and LEAVE event). Notably, engaged mice took less than half a second after the last licks to leave the site in the majority of bouts (Median time to run = 0.46 s). The running time is comparable to the licking time.
(k) Monotonic relationship between the number of consecutive failures after the last reward and the time licking after the last reward (each dot represents the means across bouts for each session).

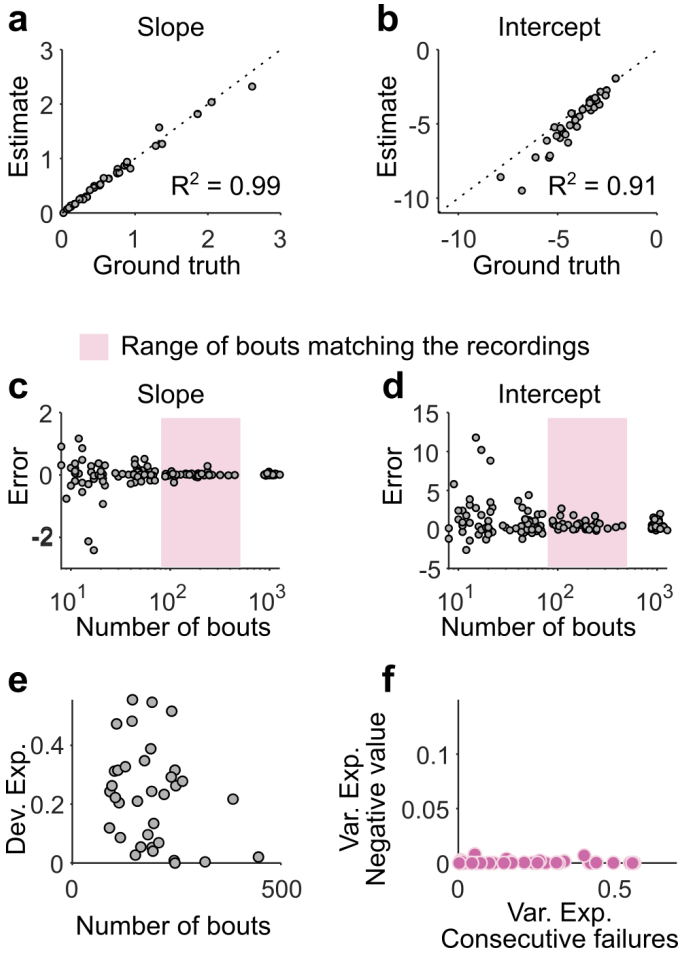

Supplementary Figure 2: Ground truth model.

(a,b) The slope (a) and intercept (b) estimates as a function of the ground truth for simulated sessions where the number of bouts matched that of real sessions. The ground truth can be recovered ($R^2 = 0.99$ for the slope; $R^2 = 0.91$ for the intercept) from the logistic regression.

(c,d) The slope (c) and intercept (d) estimates as a function of the ground truth for simulated sessions with varying number of bouts. Overall, the ground truth can be precisely recovered for sessions with more than 100 bouts.

(e) Deviance explained from a logistic regression model that fits simulated sessions using the two DVs ('Consecutive failures' and 'Negative value', same model as in Fig. 1) as a function of the number of bouts in each session. A deviance explained smaller than 1 indicates that, although the ground truth can be recovered, the leaving behavior is not deterministic and involves some stochasticity (here the variability was matched to that of the data).

(f) For all simulated sessions in (e), the variance explained by the 'consecutive failures' DV was greater than the variance explained by the 'negative value' DV, indicating that the model inferred the true DV.

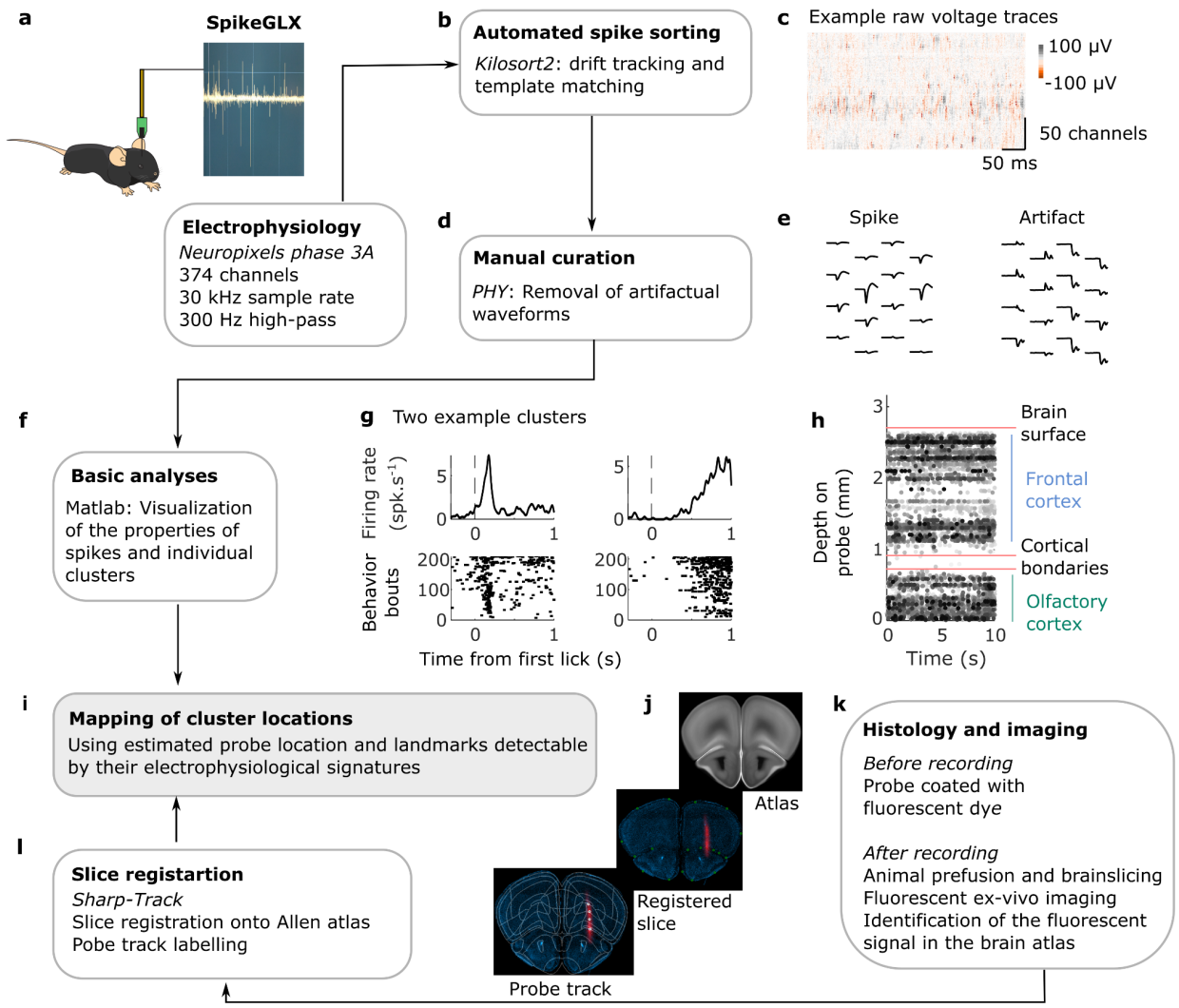

Supplementary Figure 3: Pipeline for extracellular electrophysiology, data processing and cluster mapping.

(a) Data collection from the Neuropixels probe.

(b) Kilosort2 is used to automatically match spike templates to raw data.

(c) Example of voltage data input to Kilosort2. Prior to the automatic sorting, the raw data is pre-processed with offset subtraction, median subtraction, and whitening steps.

(d) Manual quality control is done on the outputs of Kilosort2 using PHY to remove units with non-physiological waveforms (e), contaminated refractory periods, low amplitude (less than 50 µV) or low spiking units (less than 0.5 spike·s^{-1}).

(f) For further quality control, visualization of peri-event spike histograms (g, top; examples histogram aligned to first lick) or scatter plots (g, bottom; example scatter plot aligned to first lick) of single neurons are made with custom-written script in MATLAB.

(h, i) Example scatter plot of all neurons recorded simultaneously along the shank of the probe. This visualization helps delimitate landmarks based on electrophysiological signatures to map cluster locations.
(j, k, l) Landmarks derived from electrophysiological responses are validated with estimates from histology using an open-source software (SHARP-Track).

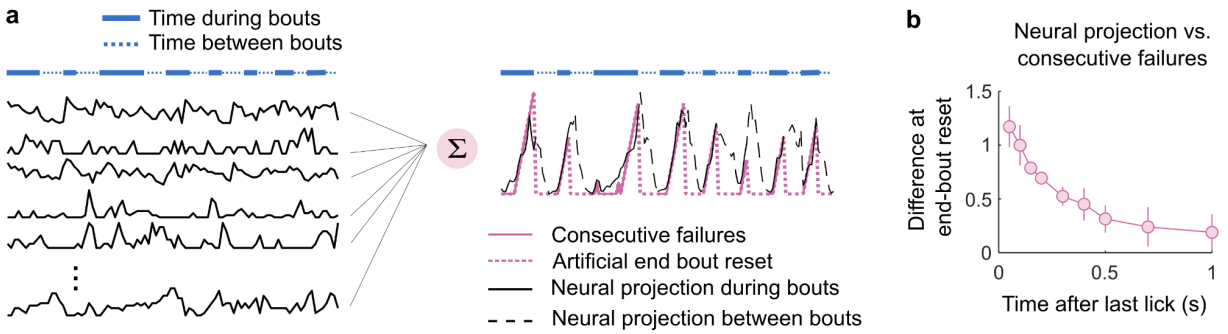

Supplementary Figure 4: Time constant of reset at the end of the bout in the frontal cortex.
(a) Example consecutive failures (pink) and neural projections (black right) of the neural activity (left, example neural traces) including the activity during 2 s after the end of each bout (dashed-line). The projection of the neural activity on the decoding weights for the consecutive failure slowly ramps down until the beginning of the next bout.
(b) To quantify the time constant of the reset at the end of the bout, the consecutive failures with an additional reset at the end of the bout were decoded from the neural activity. We considered the decoding projection at different times after the end of the last lick of bout 'n' and before the start of bout 'n+1' and plotted the difference between the number of the consecutive failures (dashed pink) and the neural projection (dashed black) at the end of each bout across recording sessions (median ± MAD; n = 11) as a function of the time after the last lick. The neural activity can reset at the end of the bouts with a time constant of around 200 ms.